Universidade de Aveiro Departamento de Engenharia Cerâmica e do Vidro
2007

Ermelinda da Conceição Portela Salgueiredo

Filmes de DLC para aplicações biotribológicas

Universidade de Aveiro Departamento de Engenharia Cerâmica e do Vidro
2007

Ermelinda da Conceição Portela Salgueiredo

DLC coatings for biotribological applications

dissertação apresentada à Universidade de Aveiro para cumprimento dos requisitos necessários à obtenção do grau de Mestre em Engenharia Biomédica – Ramo Biomateriais, realizada sob a orientação científica da Profª. Drª. Florinda Mendes da Costa, Professora Associada do Departamento de Física da Universidade de Aveiro, e sob a co-orientação científica do Prof. Dr. Rui Ramos Ferreira e Silva, Professor Associado do Departamento de Engenharia Cerâmica e do Vidro da Universidade de Aveiro

Apoio financeiro do POCTI no âmbito do III Quadro Comunitário de Apoio.

Apoio financeiro da FCT e do FSE no âmbito do III Quadro Comunitário de Apoio.

Dedico este trabalho a meu pai e minha mãe por todo o seu sacrifício e amor incondicional.

“Colhi um ramo de flores de outras pessoas; nada, além dos fios que as unem, são meus”

Michel de Montaigne, 1533-1592

o júri

presidente

Prof. Dra. Maria Helena Figueira Vaz Fernandes
professora associada da Universidade de Aveiro

Prof. Dra. Florinda Mendes da Costa
professora associada da Universidade de Aveiro

Prof. Dr. Rui Ramos Ferreira e Silva
professor associado da Universidade de Aveiro

Prof. Dra. Maria Pia de Melo Alvim Ferraz
Professora auxiliar da Faculdade de Ciências da Saúde da Universidade Fernando Pessoa

agradecimentos

Gostaria de agradecer à Prof. Dra. Florinda Costa e ao Prof. Dr. Rui Silva por me terem orientado ao longo deste trabalho e, sobretudo, pela confiança que depositaram em mim.
Ao Dr. Filipe Oliveira ("Chefe") agradeço pelo muito que me ensinou sobre Ciência e Engenharia de Materiais.
Um agradecimento muito especial à Dra. Mercedes Vila por todo o apoio técnico mas sobretudo pela amizade e constante optimismo. *Gracias guapa.*
Aos meus colegas de laboratório (o fabuloso grupo do Diamante e afins) não tenho palavras para expressar tudo o que foram para mim ao longo destes anos. Por tudo o que me ensinaram, pelo constante apoio a todos os níveis, o meu mais sentido agradecimento.
À "Banda do Zé" do Departamento de Engª Cerâmica e do Vidro quero agradecer por serem o meu porto seguro em tantas horas difíceis e também pela partilha das alegrias e conquistas. Obrigada por estarem sempre lá para mim…
À Prof. Dra. Ascensão Lopes e à Marta Silva da Faculdade de Engenharia da Universidade do Porto, agradeço todo o apoio técnico nos estudos de biocompatibilidade. Agradeço sobretudo a constante disponibilidade e carinho que me dedicaram. Agradeço também à Marta Laranjeira pela colaboração.
Ao Cristiano Abreu, do Departamento de Engenharia Mecânica da Universidade do Minho, agradeço a colaboração na caracterização tribológica deste trabalho.
À Prof. Dra. Maria Helena Fernandes e ao Dr. Pedro Gomes da Faculdade de Medicina Dentária da Universidade do Porto agradeço a colaboração na parte experimental dedicada às culturas celulares, e o apoio na interpretação e discussão de resultados.
A todos os funcionários do departamento de Engª Cerâmica e do Vidro agradeço reconhecidamente o apoio técnico e constante disponibilidade.

A todos os meus amigos e companheiros de jornada (seria impossível nomear todos) um obrigada do fundo do coração.

À Dina, Rita e Marta pelo imenso privilégio da vossa amizade.

À minha família agradeço todo o amor e paciência ao longo deste percurso.

Ao Mário agradeço por todos estes anos em que sonhámos juntos.

À minha filha Maria por me renovar a esperança a cada dia.

palavras-chave carbono amorfo, *sputtering*, nitreto de silício, aplicações biomédicas, tribologia

resumo

Os filmes de carbono amorfo tipo diamante (DLC) actuam como lubrificantes sólidos em muitas aplicações de desgaste incluindo os implantes articulares da anca e joelho. Entre estes, os filmes de carbono não-hidrogenado podem ser depositados pela técnica de deposição física em fase vapor (PVD) a baixas temperaturas (<325ºC). Estes filmes protectores são quimicamente inertes, possuem elevada dureza e baixo coeficiente de atrito contra polietileno de ultra alto peso molecular (UHMWPE) e outros biomateriais, aumentando assim a qualidade dos implantes articulares.

Filmes de DLC foram depositados por sputtering DC em substratos à base de nitreto de silício (Si_3N_4 monolítico; compósitos Si_3N_4/TiN e Si_3N_4/bioglass) visando elevados níveis de adesão. A nanoestrutura do DLC, confirmada pela fraca intensidade da banda D do espectro Raman, combinada com o elevado conteúdo de ligações sp^3, comprovado pelo desvio da banda G, levou a um valor de dureza de 16 GPa. Os filmes apresentam-se densos e homogéneos com um valor extremamente baixo de rugosidade (RMS=2.6 nm).

Antes de ser implantado no corpo humano, um material tem de provar ser biocompatível. Antes da deposição de DLC, os substratos foram recobertos com uma camada de Si para promover a adesão. Após 35 dias de imersão em SBF, a observação SEM demonstrou que não ocorreu formação de camada apatítica na superfície. A análise química por ICP-AES mostrou que não houve variação na concentração dos iões Ca e P, e que não foram libertados elementos tóxicos na solução. A hidrofobicidade, tensão superficial e carga superficial deste biomaterial foram também avaliadas. A superfície apresentou um valor ligeiramente negativo de carga, como demonstrado pelo valor do potencial zeta de -35.0 $\pm$ 1.3 mV para pH=7.4 $\pm$ 0.2. A tensão superficial foi de 45.7 mN/m, apresentando uma componente dispersiva predominante da tensão superficial. Os resultados mostram que o revestimento de DLC é tendencialmente hidrofóbico. Os estudos com a linha celular de osteoblastos humanos MG63 não revelaram indícios de citotoxicidade. As células apresentaram morfologia normal e maior crescimento celular, quando comparadas com as placas standard de cultura, mostrando, no entanto, menor adesão celular.

Para os ensaios biotribológicos, bolas e discos cerâmicos foram recobertos com filmes de DLC numa primeira etapa para ensaios de deslizamento a seco em movimento recíproco, com pares próprios. Um *bias* negativo foi aplicado ao compósito condutor Si_3N_4/TiN, resultando em valores de coeficiente de atrito extremamente baixos(μ=0.015). Numa segunda etapa, placas recobertas com DLC foram testadas contra bolas de UHMWPE. Os testes foram efectuados a seco e lubrificado (SBF). Os resultados preliminares mostram que o coeficiente de atrito mantém-se constante ao longo do ensaio, sem delaminação do DLC. Estes resultados favoráveis permitem recomendar o Si_3N_4 revestido com DLC como adequado para aplicações em próteses articulares.

keywords diamond-like carbon, sputtering, silicon nitride, biomedical applicattions, tribology

abstract

Diamond-like carbon (DLC) films act as solid-film lubricants in many wear resistant applications including articulated implants as hip and knee joints. Among these, non-hydrogenated amorphous carbon films can be grown by Physical Vapour Deposition (PVD) technique at low deposition temperatures (<325ºC). These protective coatings possess chemical inertness, high hardness and low friction coefficient against Ultra High Molecular Weight Polyethylene (UHMWPE) and other biomaterials, thereby improving the quality of articulated implants.

In this study, the DLC films were deposited by DC magnetron sputtering over silicon nitride based substrates (bulk Si_3N_4; Si_3N_4/TiN and Si_3N_4/bioglass composites) aiming high adhesion levels. DLC nanostructure, confirmed by the weak intensity of the Raman spectra D band position, combined with significant sp^3 content, as depicted by the G band downshift, lead to a hardness value of about 16 GPa. Films are dense and homogeneous in all the deposited area with an extremely low roughness of 2.6 nm (RMS).

Before implantation in the human body, a material must prove to be biocompatible. Prior to the DLC deposition, the Si_3N_4 based ceramics were coated with a Si interlayer to promote adhesion. After 35 days of immersion in Simulated Body Fluid, SBF, the DLC surface showed no signs of apatite layer formation, as observed by SEM. Also, ICP-AES analysis confirmed no variation of the Ca and P ions concentration levels, and no toxic elements released into solution were detected. Hydrophobicity, surface tension and surface charge was also evaluated. The DLC surface is slightly negative charged, has shown by the zeta potential value of -35.0 ± 1.3 mV at $pH=7.4 \pm 0.2$. The surface tension of the DLC coated samples was 45.7mN/m, presenting a dominant dispersive component of the surface tension. Results showed that the DLC coating is quite hydrophobic. Using the MG63 osteoblast-like cells, no evidence of citotoxicity was observed. Cells showed normal morphology and higher cell growth, compared to standard culture plates, although with low cell adhesion.

For biotribological assessment, in a first stage Si_3N_4 ceramic balls and discs were coated with DLC films for self-mated reciprocating dry sliding tests. A negative bias voltage applied to a conductive Si_3N_4/TiN composite showed a remarkable improvement under the same tribological solicitation, presenting very low friction coefficient values (μ=0.015) during the full duration of the test. In a second stage, DLC-coated Si_3N_4 ceramics were tested against UHMWPE spheres using a reciprocating ball-on-flat set-up. The sliding occurred under dry and lubricated (SBF) conditions. Preliminary results showed that the friction coefficient is almost constant during the running-in period without delamination of the DLC coating.

Based in these favourable results, the DLC-coated Si_3N_4 biomaterial seems adequate to be used for articular prosthesis development.

INDEX

Introduction

Nowadays, worldwide, the artificial joint market involves over $3 billion (US) annually. In the USA, for example, the number of Total Hip Arthroplasty (THA) interventions is approximately 168 000 a year, being 5-10% of this number revisions of failed implants. Thus, small improvements in the quality of these implants represent a large reduction in economical costs. Moreover, the most important factor is the improvement of the patient's quality of life. The most common cause of artificial joint failure comes from the wear debris of polymer articulating components, due to gradual roughening of metal articulating surfaces.

In this work, Diamond-like Carbon (DLC) coated silicon nitride (Si_3N_4) based ceramics were evaluated regarding biocompatibility and tribological behaviour, aiming for future application in the hip joint tribosystem.

In Chapter I a bibliographic review of the most relevant issues in DLC films over Si_3N_4 based ceramics for biotribological applications is accessible. Special emphasis is given to the magnetron sputtering technique chosen for the DLC deposition as also in bone description and biocompatibility evaluation procedures.

Chapter II is related to the evaluation of DLC coatings surface properties (zeta potential, surface tension) and citotoxicity tests using MG-63 osteoblast-like cells.

Lubricated and unlubricated reciprocating sliding experiments against UHMWPE balls were further conducted. These results and those obtained for the DLC self-mating pairs in unlubricated sliding conditions are given in Chapter III.

Chapter IV is dedicated to the microstructural characterization of a DLC-coated Si_3N_4-bioglass composite. The DLC films have the advantage of improving the surface properties of this biomaterial, acting as autolubricants while improving hardness, and also providing a higher toughness.

In Chapter V are summarized the main conclusions of the work. By looking at the favourable results, it is reasonable to say that DLC-coated Si_3N_4 materials are excellent candidates for the hip joint tribosystem.

Chapter I

Bibliographic overview

1. Carbon allotropes and amorphous carbon

1.1. Bonding in carbon: the different allotropes

The word carbon was coined in 1789 by Antoine de Lavoisier from the Latin word *carbo* (charcoal). By the end of the eighteen century graphite and diamond had been identified as forms of the same element. The third major form, the fullerenes, was only discovered in 1985 [1]. The highest strength fibers are the carbon fibers, one of the best lubricants is graphite, the strongest crystal is diamond, one of the best gas adsorvers is activated charcoal and one of the best helium gas barriers is vitreous carbon [2].

Some relevant properties and characteristics of the Carbon atom are given in Table 1 [2].

Table 1: Properties and characteristics of the carbon atom

Z (atomic number = number of protons or electons): 6
N (number of neutrons): 6 or 7 (common isotopes)
A (Z + N or number of nucleons or mass number): 12 or 13
Atomic mass: 12.01115 amu
First Ionization Potential: v = 11.260
Quantum number of last added electron: n = 2, l = 1
Outermost occupied shell: L

The element carbon is placed in the first full row of the Mendeleïev Table and exhibits unique bonding possibilities ($1s^2$, $2s^2$, $2p^2$). When a carbon atom reacts with other carbon atom (hybridization), exciting a 2s electron into a empty 2p orbital, this can happen in three different ways originating the hybrid orbitals sp^3, sp^2 and sp^1, corresponding to triple, double and single bondings, respectively.

The properties of carbon-based materials depend of their electronic configurations. The main feature is the multiple bonding available with catenation (carbon atoms can bond with each other) of carbon through the p-orbitals and two principal regimes: either a single σ-bond, as in diamond or aliphatic chains, or a double bond (σ- and π-bonds) as in graphite and graphitic compounds [1].

1.1.1. Diamond structure

Diamond is a metastable form of carbon at room temperature. In the absence of air, diamond heat-treated to 1000 ºC becomes covered with a layer of graphite. Due to its high density, diamond is the stable form at high pressure (d=3.51 $g.cm^{-3}$ in comparison to 2.26 $g.cm^{-3}$ for graphite or 1.72 $g.cm^{-3}$ for solid fullerenes). Graphite is stable at low and medium pressures.

Solids with only σ-bonds form 3D structures which are rigid and isotropic. The allotropic form is diamond with four equal hybridized sp^3 molecular orbitals. Each C atom is covalently attached to four atoms in tetragonal bonds of 1.54 Å long creating a cubic structure, as shown in Figure 1. Diamond has the highest atomic density of any solid, is the hardest material known, has a very high thermal conductivity and the highest melting point. It is an insulator with a reported band gap as high as 5.5 eV [1].

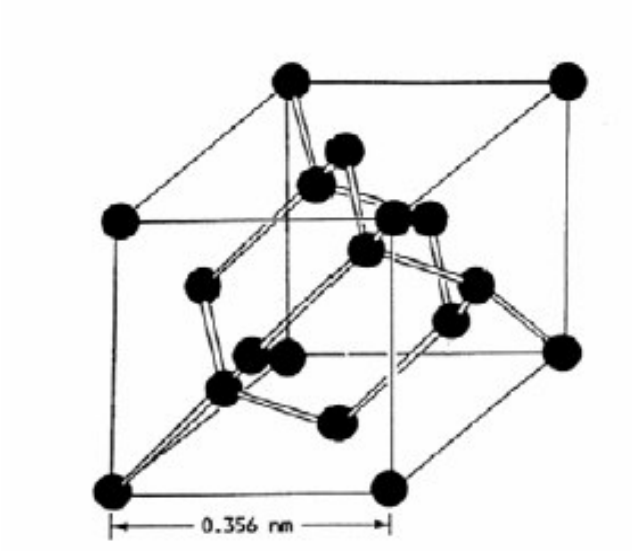

Figure 1: Structural unit of diamond [1]

1.1.2. Graphite structures

The trigonal sp^2 bonding of carbon atoms is present in graphite, whose structure is shown in Figure 2.

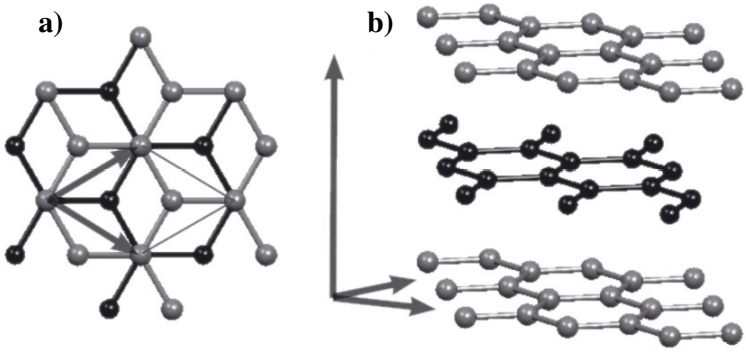

Figure 2: Graphite lattice in top (a) and side (b) view [3]

In graphite, the association of σ- and π-bonds in he graphitic arrays of atoms results in layered structures with a high degree of anisotropy. Graphite in-plane exhibits even a higher thermal conductivity than diamond. In graphite the band-gap is 0.04 eV. Graphite is a semi-metal with a high electrical conductivity, similar to that of iron at room temperature [1].

1.1.3. Fullerenes

Fullerene, the molecular allotrope of carbon, is a cage molecule, being the largest molecule ever seen in nature, containing 60 carbon atoms, as represented in Figure 3. In fullerenes occurs a re-hybridization due to the bending of the graphitic bond: these are the $sp^{2+\varepsilon}$ forms, intermediate between sp^2 and sp^3.

Figure 3: Schematic of a C_{60} fullerene molecule [2]

1.1.4. Other Carbon Allotropes

A total of dozen different allotropic forms of carbon structures are known. Our interest is focused in the amorphous carbon allotrope, as follows.

1.2. Diamond-like carbon, DLC

DLC films are metastable amorphous materials that can sometimes include a microcrystalline phase. It can be defined as an amorphous carbon material that contains a mixture of sp^3, sp^2 and sp^1 hybridized carbon. These hybridized forms are present in the DLC films as a disordered network, schematically represented in Figure 4 [4]. Usually, DLC contains a significant fraction of sp^3 bonds [5].

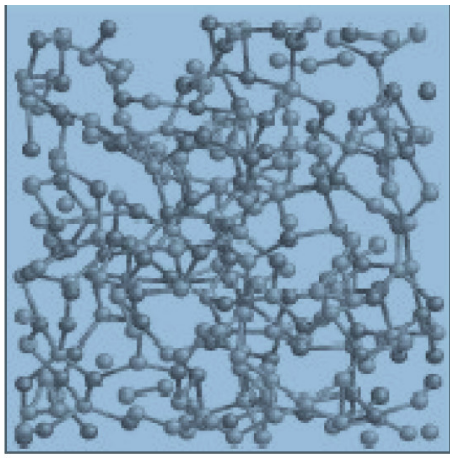

Figure 4: Structural model of Diamond-like Carbon [4]

DLC films have been first deposited by Aisenberg and Chabot in 1971. Since then, DLC films have been deposited by several methods like DC or RF-plasma assisted Chemical Vapour Deposition (CVD), sputtering, ion beam deposition, among other methods, using solid or gaseous carbon source materials. The term “diamond-like” is used due to the similarity in terms of hardness and optical gap between this disordered form of carbon and diamond. This material can be deposited at substrate temperatures below 325 ºC, and the ion bombardment of the growing film is essential for obtaining the diamond-like properties [4].

The composition of the DLC films can be organized in a ternary phase diagram of sp^3 and sp^2 ratios, and the hydrogen content of the coating, as shown in Figure 5. The sp^2 bonded graphitic carbon lies in the lower left-hand corner. Phases with high hydrogen content form an interconnected molecular structure and lie at the low right-hand corner of the diagram. The typical hydrogenated amorphous carbon (a-C:H) coatings are situated in the middle of the diagram, showing a varying ratio of sp^3/sp^2 bonding and hydrogen content. The tetrahedral amorphous carbon (ta-C) coatings are situated on the left side depending on the ratio of sp^3/sp^2 bonding [5].

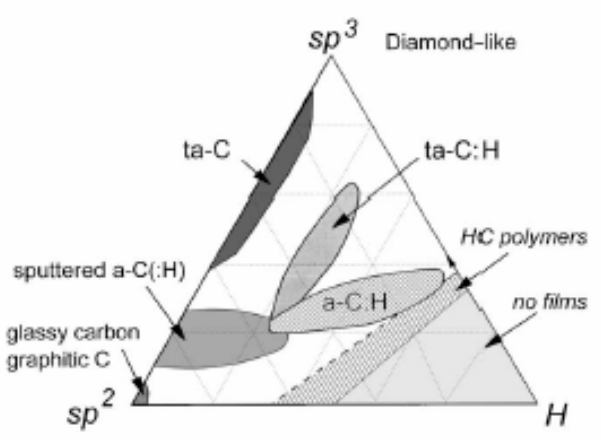

Figure 5: Ternary phase diagram of sp^3, sp^2 and hydrogen content of various forms of DLC [5]

1.2.1. Hydrogenated Diamond-like carbon

Depending on the precursor material, hydrogen is present in a large amount of DLC films. The percentage of hydrogen can vary from smaller amounts ~10% to 60%, depending on the deposition method. Hydrogen is added to the precursor gas aiming to obtain a wide optical gap and high electrical resistivity, because it passivates the dangling bonds in the amorphous structure [4].

The main advantage in employing hydrocarbon gases (a-C:H) is the high deposition rate. But hydrogen-free DLC has several advantages over hydrogenated DLC, such as higher hardness, elastic modulus and consequently better wear resistance, lower coefficient of friction and higher thermal stability [6].

Some relevant differences between graphite, diamond and DLC are summarized in Table 2.

Table 2: Comparing graphite, diamond and DLC [2,5]

	Graphite	**Diamond**	**DLC**
Composition	Pure carbon	Mostly carbon (<1 at % hydrogen)	0 – 60 at. % hydrogen
Microstructure	Crystalline	Crystalline	Amorphous
Atom-bonding state	sp^2 only	sp^3 only	sp^2, sp^3, sp^1 (variable ratio)
Stability	Stable	Stable at high temperature and high pressure	Metastable
Raman Spectrum	Sharp peak at 1580 cm^{-1}	Sharp peak at 1332 cm^{-1}	Broad humps at 1330 and 1550 cm^{-1}
Electrical conductivity	Conductor (*ab* direction)	Insulator	Insulator
Density ($g.cm^{-3}$)	2.267	3.515	1.2 – 2.4
Gap (eV)	~ 0	5.5	0.4 – 2.5
Hardness (GPa)	-	100	3 - 80

1.2.2. DLC properties and applications

Besides the properties already referred in Table 2, DLC also presents low friction coefficient, with values as low as 0.01 for a-C:H in a vacuum. The friction coefficient increases with increasing humidity reaching values of 0.28. DLC possesses high optical transparency over a wide spectral range, high electrical resistivity and chemical inertness both to acids and alkalis. DLC films high hardness and chemical resistance turns them suitable for use as wear-resistant coatings on different substrates, namely metals, and on optical and electronic components [4].

Mechanical properties are very important for the use of DLC as a protective coating. ta-C films hardness is similar to that of diamond, being interesting for use in MEMs instead of polysilicon. DLC has the advantage of being amorphous with no grain

boundaries, resulting in very smooth films, contrarily to CVD polycrystalline diamond.

DLC can be deposited at room temperature, which is a great advantage for use in temperature sensitive substrates, such as plastics. Due to their good coverage, DLC films act as good corrosion barriers, fundamental for coating disks and recording heads in the magnetic storage technology.

The disadvantages of DLC films are their intrinsic stress and thermal stability. The compressive stress limits the maximum thickness of adhesive films. Maximizing the hardness is also maximizing the stress, thus minimizing the thickness of an adherent layer. It is therefore fundamental to ensure a good adhesion between the film and the substrate. One way to contour this problem is by depositing a carbide-forming adhesion layer, such as Si, Cr or W, before depositing carbon.

DLC films are of growing interest as coatings in hip joints, heart valves and stents due to their low friction coefficient and the fact that, being a carbon material, it is biologically compatible and it does not produce metallic wear debris [5].

1.2.3. Biomedical applications of DLC

The *in vivo* biocompatibility of DLC was preliminarily tested in sheeps using DLC coated orthopaedic pins, aiming to study the soft tissue retraction around the pins. Apparently, the DLC coated pins reduced the problems of tissue retraction and subsequent infection [7].

Several studies report the biocompatibility of DLC coatings, as the work of Cui and Li. [8] Butter *et al* [9] used human cell lines (human synovial fibroblasts (HSFs) and human osteoblast-like cells (SaOS-2) or murine cell lines (IC-21)) and no signs of film toxicity were revealed. Allen and co-workers [10] used MG-63 and SaOS-2 cell lines in DLC coated polystyrene substrates. Analysing the culture medium and cell lysates, the cells maintained an osteoblastic phenotype, with expression of alkaline phosphatase, osteocalcine and type I collagen, showing DLC biocompatibility *in vitro*. The DLC-coated cobalt-chromium cylinders implanted on intramuscular locations on rats were retrieved 90 days after surgery and showed that the DLC specimens were well tolerated by the organism. The implants were surrounded by a thin fibrous membrane with no evidence of

acute inflammatory reaction or cellular necrosis, presenting the typical behaviour of a inert biomaterial.

DLC-coated steel fracture fixation rods were implanted in a human body for 7 months and were found to prevent rod corrosion and metal ion release, and improving the wound healing time [11].

DLC coatings are hard, possess a very low surface roughness, are bioinert and prevent the leaching of metallic ions into the body. This set of properties makes them adequate for biomedical applications, like orthopaedic and cardiovascular components, guidewires, ophthalmic and biosensors [11-13]. In total hip and knee arthroplasties, the load-bearing surfaces are submitted to wear, originating polyethylene debris that are phagocytosed resulting in granulomatosis lesions, osteolysis and bone resorption, causing pain and aseptic loosening of the prosthesis. DLC coatings may offer a solution to these problems, reducing the wear of polyethylene compared to the values obtained for ceramics such as alumina and zirconia [12,13].

2. DLC deposited by sputtering

2.1. Sputtering technique

Although the production of thin films by ion bombardment from a plasma source is known since the beginning of the previous century, it was only after the 70's that it became a largely used technique. The development of integrated circuits who demanded more reliable alternatives to thermal evaporation, and the development of new methods for plasma formation based on the application of magnetic fields were decisive for the wide spread implementation of the sputtering technique.

Basically, the sputtering technique is based on the intense bombarding of a material with ions produced in an electric discharge in the form of plasma, from a solid surface. When the energy of the ions is high enough, the interaction with the surface of the material (through the exchange of the kinetic moment) originates the pull out of the surface atoms that pass to the vapour state [14].

Schematically, there are four major steps in the sputtering process [15]:

Electric discharge between two electrodes:

cathode and an inert gas (Argon)

⇩

Ion acceleration towards the cathode and

bombarding of the surface

⇩

Transfer of the kinetic moment

⇩

Target atoms condense in the substrate surface

The sputtering technique is probably one of the most widely used deposition processes, not only in laboratories, but also at an industrial level. The sputtering process is schematically described in Figure 6. Ar-ions are accelerated towards the target material coupled to a negative potential, which subsequently knock out target atoms that condense on the substrate surface.

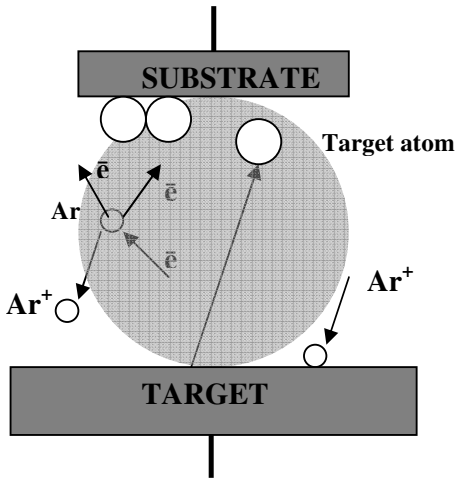

Figure 6: Schematic representation of a sputtering process

The most fundamental parameter in the sputtering process is the *sputter yield*, which is defined as the number of atoms or molecules ejected from a target surface per incident ion and is a measure of the sputtering efficiency [14].

The sputtering technique presents several advantages, such as [15]:

- Low temperature deposition;
- Versatile technique for the evaporation of distinct materials such as metals, ceramics, and even materials with a high melting point;
- Good adhesiveness of the deposited film due to the high energy of the deposited atoms on the substrate;
- Easiness on the control of the deposition rate, mainly by controlling the power applied in the discharge.

2.1.1. Sputtering types

DC Sputtering

The deposition process in a DC magnetron sputtering is described above. This type of magnetron sputtering is used to deposit thin films in conducting materials, such as metals [15].

RF sputtering

In continuous current it is very difficult to deposit in isolating materials, due to the accumulation of positive ions originated by the bombarding of the target. This drawback can be solved by using an alternate current of high frequency – RF sputtering – in which the accumulated positive charge disappears by reversing the polarity in each semicycle. Using this method it is possible to deposit the films in isolating substrates, as well as in conductor and semiconducting ones.

The fundamental principles of RF sputtering are based in the different response of ions and electrons in the plasma to highly energetic magnetic fields. The typical operation frequency of most RF sputtering apparatus is 13.56 MHz, used in both scientifically and industrial applications.

The main drawbacks of this technique are the complexity in operating at high alternate currents and the high cost of the power supply [15]. Also, the deposition rates are usually low and the process is difficult to scale up for commercial applications [16].

Bias-assisted sputtering

In this method, electric fields near the substrate are modified in order to vary the flux and energy of incident charged species. This is obtained by applying a negative DC or RF bias to the substrate. The values typically used are of -1000 to -3000 V in the target voltages and bias voltages of -50 to -300 V.

Bias sputtering is an effective process in altering some properties in the deposited films, such as [14]:

- Resistivity – significant reduction in resistivity, specially in metal films;
- Hardness and residual stress – increased (or decrease) hardness with magnitude of the negative bias voltage applied, with similar behaviour for the residual stress;
- Film morphology - the columnar microstructure of RF-sputtered films (such as Cr) is totally disrupted by ion bombardment and replaced by a compacted, fine grained structure;
- Density – increase in film density;
- Adhesion – film adhesion is often improved by ion bombardment of the substrates during initial stages of film formation.

Reactive sputtering

This technique uses a continuous current in the presence of a reactive gas and it is usually employed for depositing metallic oxides. The reactive atmosphere changes the discharge conditions, because it doesn't only interact with the material that condenses over the substrates, but also with the target material.

The advantages of this technique are the use of a continuous current power supply and the easy implementation at an industrial level. It is widely used for depositing TiN in microelectronic devices and protective coatings in mechanical pieces based on nitrides, carbides and some transition metals [15].

The main disadvantage is the arc events. During deposition some areas on the target become covered with an insulating layer, as do the target earth shields. This process in which the target is covered with the reaction product is called "target poisoning". The poisoned layers charge up until breakdown occurs in the form of an arc. These events

promote the ejection of droplets of material from the target surface, originating defects in the film surface [16].

2.1.2. Magnetron Sputtering sources configuration

The magnetron sputtering technique is widely used nowadays in an industrial level to deposit hard, wear-resistant coatings, and also coatings that are corrosion resistant and with specific optical or electrical properties.

In the conventional sputtering technique, the plasma is strongly confined to the target region. In this way, only substrates that are positioned inside this region suffer ion bombardment, resulting in a great difficulty to produce fully dense quality coatings in large and complex components [16].

Magnetron sputtering has overcome the limitations of the basic sputtering process, who presented low deposition rates, low ionization efficiency in the plasma and high substrate heating effects. This is achieved by adding magnetic fields parallel to the target surface, which forces the electrons to extend their dwell time in the plasma and cause further ionization and a higher plasma density. The higher plasma will give a denser sputtering and an increased deposition rate [16,17].

Compared with Arc-evaporation and Plasma Enhanced Chemical Vapour Deposition (PECVD), the ion-bombardment of the substrate is quite limited in a sputtering process. But, recent progresses in magnetron sputtering have increased the ion bombardment, using the technique of unbalanced magnetron sputtering, UMS [23,24].

But it is difficult to deposit uniform coatings onto complex components using a single magnetron source. So, aiming for commercial applications, a number of multiple-magnetron systems have been introduced, in a process called closed-field unbalanced magnetron sputtering, (CFUMS) [15].

These systems are ideal for the deposition of alloy nitrides, because each of the magnetrons can be of a different material and by sputtering the targets at different rates, any required alloy composition can be obtained. The deposition of coatings with graded properties is also possible and with an excellent coating-to-substrate adhesion [16,17].

The application of pulse power to the target and the substrate in a magnetron system alters the homologous temperature, the ratio of the fluxes of bombarding ions and

deposited atoms and the energy of the bombarding ions, which are the most important parameters in a sputtering process, resulting in better coating properties. [18]

Pulsed magnetron sputtering (PMS), using a medium frequency range (10-200 kHz), is used for depositing insulating films, significantly reducing the formation of arcs. Deposition rates obtained by PMS are very high allowing the deposition of defect-free ceramic films. Thus, PMS induced a substantial commercial interest, leading to the development of a new generation of magnetron power supplies and pulse units. [16,18]

2.2. DC and RF magnetron sputtering of DLC

Among the extense work found in literature on DLC deposited by DC or RF magnetron sputtering, the work of the following authors is worth of note.

Zhang and co-workers [19] deposited hydrogen free amorphous carbon coatings on steel substrates by DC magnetron sputtering, with bias in the range of -20 to -150 V. Increasing bias voltage resulted in increased coating hardness and surface smoothness, but with lower adhesion and higher coefficient of friction. The balance may be in bias–graded deposition (gradually increase the bias power during deposition) to produce high adhesion and high hardness coatings.

Logothethidis and Gioti [20] deposited amorphous carbon films on Si wafers by RF magnetron sputtering, resulting in films with high sp^3 content. They also studied the effect of bias voltage applied during deposition in the level of stress: for zero or positive bias voltage values the films have a varying sp^3 and sp^2 fraction, while a negative bias leads to the growth of films rich in sp^3, but with high internal stresses.

Chowdhury and co-workers [21] used RF sputtering and substrate temperature to deposit DLC on silicon wafers (1 0 0), showing that substrate temperature has a strong influence on the bonding properties of the deposited films and the changes in bonding ratio (sp^3/sp^2) with correlation in the obtained mechanical properties. Hardness and Young's modulus increased with increased temperature up to 125 ºC and then decreased.

Andújar *et al* [22] studied the effect of Argon gas pressure and RF power in the DLC films deposited by sputtering on silicon substrates. At constant power, the increase in pressure leads to smaller deposition rates and compressive stress, with increased sp^2 phase. The increase in RF power, at constant pressure, increases the deposition rate and a reduction in compressive stress.

3. Ceramics

Ceramics are generally obtained from the application of pressure and heat to inorganic base powders. These materials have a wide range of applications, from building blocks to devices used in medicine.

Ceramics have an exceptional compressive strength, but are very brittle and weak in torsion and bending. Their coefficient of thermal expansion and self-friction coefficient are lower than those of metals, which means lower running temperatures and less consumption of lubricant. Ceramic parts can be produced in various ways. Their manufacture can be by mechanical pressing, extrusion or slip casting. Once compacted, the material is sintered to bring out the full physical, mechanical, chemical and temperature resistant properties [23].

Conventional ceramic materials consist mostly of oxides, which are mainly ionic materials. The bondings are nondirectional and the densification of these ceramics occurs by volume or grain boundary diffusion, enhanced by vacancy formation, due to non-stechiometry. In other ceramics, like silicon nitride (Si_3N_4), the highly covalent and strongly directional chemical bondings cause very low self-diffusion coefficients. Therefore, the conditions for the bulk diffusion are unfavourable and sintering of covalent substances is usually difficult [24].

3.1. Silicon nitride ceramics

Silicon nitride ceramics is a generic designation that covers a variety of grades of Si_3N_4 based materials, which incorporate additional compounds necessary for the complete densification of the Si_3N_4 starting powder. These are heterogeneous, multicomponent materials characterized by the inherent properties of the crystalline modifications α and β of Si_3N_4 and the significant influence of the densification additives [25].

Properties and applications

Metals in the annealed state are ductile materials and can usually be readily net-shaped by cold-working, which provides, at the end of the forming step, a material with improved mechanical resistance. Silicon nitride ceramics have been developed for use at

higher temperatures than those allowed by metallic superalloys [26]. Specifically, silicon nitride was developed for use in gas turbines that operated at elevated temperatures and to obtain greater efficiencies in space, automotive and electric power generating applications [27].

Silicon nitride is a ceramic material that possesses an outstanding set of chemical, physical and mechanical properties [24,25], such as: wear and corrosion resistance, high temperature stability, resistance to thermal shock, high hardness and fracture toughness, chemical inertness, low friction coefficient and resistance to oxidation. Some properties of the Si_3N_4 ceramics are shown in Table 3 [25].

Table 3: Properties of the Si_3N_4 ceramics [25]

Electrical resistivity	$> 10^{14}$ Ω.cm
Linear thermal expansion coefficient, α	$2.8 – 3.6 \times 10^{-6}$ K^{-1}
Mechanical strength, σ	800 – 1400 MPa
Fracture toughness	3 – 12 $MPa.m^{1/2}$
Hardness	12 – 20 GPa

Due to this unique set of properties, Si_3N_4 can be used in a wide range of applications [24,25], namely:

- Cutting tools;
- Ball bearings and sealing;
- Engines components;
- Metal forming and processing devices;
- Gas turbines;
- Automotive industry (Fuel injector parts, turbocharger rotors,…);
- Aircraft engines (ceramic turbine nozzles, cutter pins,…);
- Space technology (turbo pump of the space nozzle, radar windows for rockets);
- Household (cooking plates with integrated heater).

Because of silicon nitride mechanical strength at elevated temperatures, it appears to be a good candidate for tribological applications such as roller bearings, presenting a better behaviour than those of steel [28]. A drawback in the application of silicon nitride parts is that they can not be applied in oxidizing environments, for temperatures above 1200-1300 ºC. Above these temperatures, the material creeps and oxidizes, even in the bulk, because the sintering aids (like MgO, Al_2O_3 or Y_2O_3) react with SiO_2 that is formed during the oxidation reaction, originating low viscous silicates [24].

Crystalline structures and correlated properties

Silicon nitride has the composition Si_3N_4 with a predominant covalent bonding (70% covalent) with a density of 3.19 $g.cm^{-3}$ [24,25]. There are known three crystalline modifications of Si_3N_4: α-Si_3N_4, β-Si_3N_4, produced under normal nitrogen pressure, and γ-Si_3N_4 which is originated at high temperature and pressure.

The α modification is dominant in the commonly produced Si_3N_4 powders. The lattice parameters of the α phase depend on the content of oxygen dissolved in the structure. The melting point of α-Si_3N_4 was observed under a nitrogen pressure of 120 MPa and a temperature of 2560 K.

The β modification is the main constituent of most Si_3N_4 ceramics. The atomic coordinates in the unit cell are kept almost constant up to 1633 K. The solubility of oxygen in the β structure can reach a maximum of 0.258% in the absence of other elements. The crystal structure of α-Si_3N_4 and β-Si_3N_4 is represented in Figure 7.

The cubic γ modification was registered under a temperature higher than 2000 K and a pressure of 15 GPa, using the laser heating technique in a diamond cell. In fact, this modification is often designated as the c-modification, in comparison to cubic boron nitride (c-BN) [24].

This cubic modification was reported in 1999 by Zerr *et al* [29], with results showing that this structure was metastable at ambient pressure, for a temperature that could go up to 700 K.

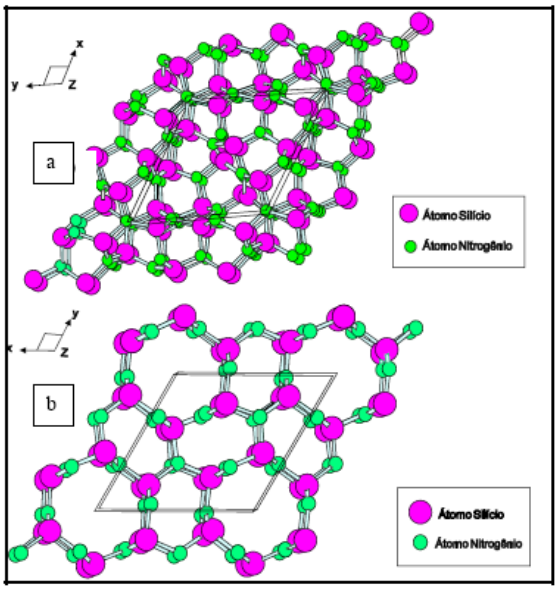

Figure 7: Crystal structure of α-Si_3N_4 (a) and β-Si_3N_4 (b) in a view nearly along the z-axis [24]

Sintering Additives

Si_3N_4 possesses a covalent bonding and has low diffusivity, so it can not be densified by solid state sintering. Thus in order to create a liquid-phase sintering process aiming for full densification, the addition of sintering aids is necessary [25].

Almost all the commercial grades of silicon nitride are made with sintering aids that support the liquid-phase sintering at temperatures ranging from 1825 ºC to 2080 ºC. A nitrogen atmosphere at moderate pressure (1-8 MPa) is used to avoid the decomposition of silicon nitride at these temperatures.

The mechanical properties at high temperatures of silicon nitride depend on the amount and composition of the sintering aids. A refractory sintering aid must be used because the sintering aids soften at a lower temperature than the silicon nitride grains. One example is the rare earth yttrium oxide, which forms high temperature eutectics. If the applications are at lower temperature, toughness and strength can be improved by *in situ* toughening, using sintering aids like Al_2O_3, MgO and CaO that cause the grains of silicon nitride to grow in length in order to increase their aspect ratio.

The high toughness is obtained by debonding along the silicon nitride grains during fracture, consequently promoting bridging across the propagating track [27].

Densification methods and mechanism

Gas-pressure sintering is the most common densification method, guarantying better reproducibility and improved properties, compared to pressureless sintering, although with a small increase in production costs. The first dense Si_3N_4 ceramics were produced using the hot pressing technique. Hot isostatic pressure, HIP, is a very high-cost technology in which the full densification of the Si_3N_4 occurs inside gas-tight glasses that soften at the sintering temperature transmitting the external gas pressure to the powder compact.

As mentioned above, full densification of the Si_3N_4 requires sintering additives. Their role is to react with Si_3N_4 and its adhered silica to produce a liquid at high temperatures, which allows mass transport through solution-reprecipitation to consolidate the solid silicon nitride by rearrangement and coalescence in equilibrium with the liquid.

The general reaction can be described as follows [25]:

a) α / β-Si_3N_4 + SiO_2 + additives (starting powder mixture)
   ↓ sintering temperature
b) α / β-$Si_3N_{4\,SS}$ + liquid of SiO_2, additives and dissolved Si_3N_4
   ↓ cooling
c) β-$Si_3N_{4\,SS}$ + amorphous phase (SiO_2, additives)
   ↓ devitrification temperature
d) β-Si_3N_4 + secondary phases + amorphous phase

3.2. Bioceramics

Ceramics have been widely used to improve the quality of life in humans, using specially designed and fabricated ceramics for the repair and reconstruction of diseased, damaged or “worn-out” parts of the body. The ceramics used to this purpose are called bioceramics. Most clinical applications of bioceramics include the repair of the skeletal system, composed of bones, joints and teeth and to augment both hard and soft tissues. They can also be used in heart valves [30].

Also, ceramics, glasses and glass-ceramics are used in medicine for eyeglasses, diagnostic instruments, chemical ware, thermometers, tissue culture flasks and fiber optics for endoscopy [31]. In many applications, ceramics are used in the form of bulk materials with a specific shape, called *implants*, *prostheses* or *prosthetic devices*. Some bioceramics applications are resumed in Figure 8 [32].

Bioceramics are made in many different configurations. They can be single crystals (sapphire), polycrystalline (alumina or hydroxyapatite), glass (Bioglass®), glass-ceramics (A/W glass ceramic) or composites (polyethylene-hydroxyapatite). Sapphire is used as dental implant due to its high strength. A/W glass-ceramic is used to replace vertebrae because offers high strength and bonding to bone. Bioactive glasses have low strength but bond rapidly to bone, being used to augment the repair of bone defects [30].

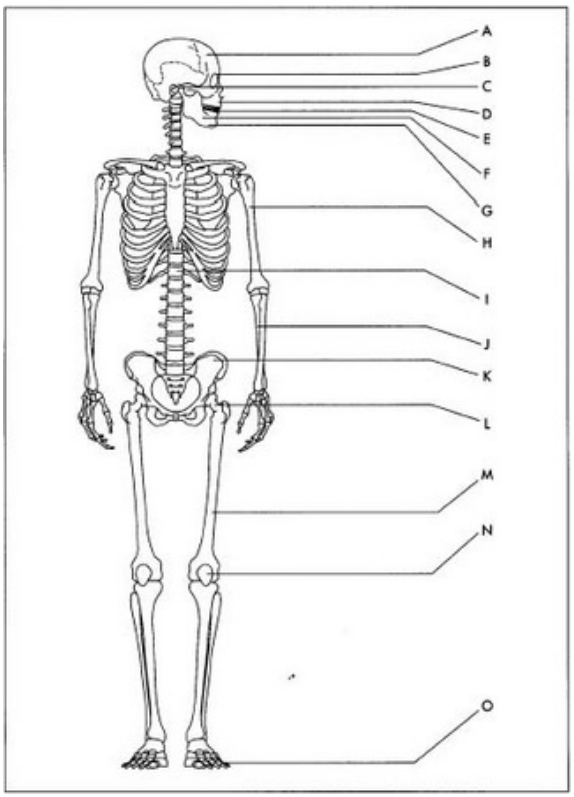

Figure 8: Bioceramic applications. A. Cranial repair. B. Eye lens. C. Ear implants. D. Facial reconstruction. E. Dental implants. F. Jaw augmentation. G. Periodontal pockets. H. Percutaneous devices. 1. Spinal surgery. J. Iliac crest repair. K. Space fillers. L Orthopedic support purposes. M. Orthopedic fillers N. Artificial tendons. 0. Joints [32]

3.2.1. Bioceramic – Tissue Interfaces

Tissue Engineering can be defined, according to Langer and Vacanti, as *"an interdisciplinary field of research that applies the principles of engineering and the life sciences towards the development of biological substitutes that restore, maintain and improve tissue function"* [33].

It is fundamental to understand that no material implanted in living tissues is inert, as all materials elicit a response from the host tissue, and that no material is suitable for all biomedical applications [30,31]. The success of ceramic, glasses and glass-ceramics depends on achieving a stable attachment to the connective tissue.

The consequences of Implant-Tissue interactions are summarized in Table 4.

Table 4: Consequences of Implant-Tissue interactions [30]

Implant-Tissue Reaction	Consequence
Toxic	Tissue dies
Biologically nearly inert	Tissue forms a non-adherent fibrous capsule around the implant
Bioactive	Tissue forms an interfacial bond with the implant
Dissolution of implant	Tissue replaces implant

All implant materials must avoid a toxic response that kills cells in the surrounding tissues or releases chemicals that can migrate within tissue fluids and cause systemic damage to the patient. One of the key reasons for choosing ceramics is their lack of toxicity.

The most common response of tissues to an implant is the formation of a non-adherent fibrous capsule. The fibrous tissue is formed to serve as a wall or isolate the implant from the host, and can, with time, lead to the complete encapsulation of the implant inside the fibrous layer. This happens with metals and most polymers.

The bioactive response occurs when a bond forms across the interface between the implant and the tissue. The interfacial bond prevents motion between the two materials and mimics the type of interface that is formed when natural tissues repair themselves.

The bioactive interface changes with time, as do natural tissues, which are in a state of dynamic equilibrium.

When the rate of change of a bioactive interface is sufficiently fast, the material "dissolves" or "resorbs" and it's replaced by the surrounding tissues. As a result, a resorbable biomaterial must have a composition that can be degraded chemically by body fluids or it can be digested easily by macrophages. The degradation products must be chemical compounds that are not toxic and can be easily disposed of without damaging the cells [30].

Synthetically, there are four types of ceramic-tissue attachment [31]:

1. Nearly inert: dense, non-porous, nearly inert ceramics attach by bone growth into surface irregularities by cementing the device into the tissues or by press-fitting into a defect (termed "morphological fixation"). Examples are single crystal or polycrystalline Al_2O_3 and Zirconia.
2. Porous: for porous inert implants, bone ingrowth occurs, mechanically attaching the bone to the material (termed "biological fixation"), as for Hydroxyapatite-coated porous metals.
3. Bioactive: dense, nonporous surface-reactive ceramics, glasses and glass-ceramics attach directly by chemical bonding with the bone (termed "bioactive fixation). Examples: Bioactive glasses, bioactive glass-ceramics, Hydroxyapatite.
4. Resorbable: dense, nonporous or porous resorbable ceramics are designed to be slowly replaced by bone, such as Calcium Phosphate, Tricalcium Phosphate, Calcium Phosphate salts.

3.2.2. Bioglass®

Due to its utilization in the experimental part of this thesis, in combination with a Si_3N_4 ceramic to form a biocomposite, it is of interest to refer the bioactive glass Bioglass®.

At the end of the 60's and beginning of the 70's Pantano *et al.* and Hench started the development of bioactive glasses for the replacement of bone in human medicine. As

regards bioactivity, Hench (1991) achieved better results developing bioactive glasses of the system SiO_2–CaO–Na_2O–P_2O_5, including the Bioglass® 45S5 (wt%: 45 SiO_2, 24.5CaO, 24.5Na_2O, 6P_2O_5). Hench and Cao and Hench described the bioactive properties of Bioglass® in 11 stages. They attributed particular significance to SiO_2 and its silicate structure, such as the [≡Si-OH] groups. Their significance begins with the initial reaction process and goes through the entire reaction for the formation of bone structure. Then, a SiO_2 gel layer forms on the surface of the glass. After the formation of this layer, an amorphous calcium phosphate can be precipitated on it. These phosphates are transformed into hydroxi-carbonate apatite. This type of apatite bonds to the living bone. It is important to refer that up to the formation of a new, mature bone structure, biological cells must be active in the kinetic stages up to stage 11, as shown in Table 5 [34].

Table 5: Interfacial reactions present in bonding between tissue and Bioglass® [34]

Stage	Process
1 e 2	Initiation and formation of ≡ Si-OH on the surface of bioactive glass
3	Policondensation of ≡ Si-OH + ≡ Si-OH → ≡ Si-O-Si ≡
4	Adsorption of amorphous $Ca^{2+} + PO_4^{3-} + CO_3^{2-} + OH^-$
5	Crystallization of HCA (Hidroxy-carbonate apatite)
6	Adsorption of biological moities in HCA layer
7	Action of macrophages
8	Attachment of stem cells
9	Differentiation of stem cells
10	Generation of matrix
11	Crystallization of matrix

4. Hip prosthesis

4.1. Historical overview

The employment of extraneous materials as surgical implants is not new, having been found reports from the pre-Christian era. Historical overviews on this matter can be found in selected publications [35-37].

In 1880, Gluck applied an ivory prosthesis by using colophony-based cement for anchorage. In 1902, Jones interposed a gold capsule between the articular heads, which had a long-term success. The first metal prostheses made of Vitallium (cobalt-chromium alloy) were produced by Bives-Wills in 1938 and by Bursch in 1939. Bursch used a self-polymerizing methyl methacrylate for their fixation. By the end of 1960 there was a widespread use of polyethylene, PE, which was introduced in 1951 by Scaglietti. Since Lavor-Gnin proved that PE had a carcinogenic power that could be harmful in a long time application, Boutin (1972) decided to use materials that presented no particular biological drawback, such as Al_2O_3, ZrO_2 and calcium aluminate. Using dense Al_2O_3 the prostheses showed very favourable results and were thought to be everlasting. Nicolini (1973) used glass-ceramics, which had many characteristics that presented better results than the materials used until then.

In 1960 Charnley developed a “low friction arthroplasty” device using shells of polytetrafluorothylene (PTFE) or Teflon, on the femoral and acetabular sides, which caused almost immediate failure due to massive debonding and wear debris. Charnley replaced the PTFE by high-density polyethylene, which was not as friction-free as Teflon but was 1000 times more resistant. This prototype was the basis for future designs, which remains the most popular form of total hip arthroplasty (THA) performed today.

Current THA is normally of titanium or cobalt-chromium alloy femoral stem cemented with poly(methyl methacrylate) (PMMA), or press-fit into place, connected to a cobalt-chromium alloy or ceramic head that articulates on a ultrahigh-molecular-weight-polyethylene (UHMWPE), or a ceramic acetabular cup fitted into a titanium or cobalt-chromium cup liner that is cemented, screwed or press-fit into place.

The prosthetic implants must fulfil two criteria. The first is biocompatibility and the second is demonstration of appropriate functional characteristics. The implant must perform as the tissue for which it substitutes [37].

Bone at the interface with an implant is often structurally week due to disease or ageing. The quality of bone in that area can deteriorate even more due to the presence of the implant or the method of fixation. Localized death of bone can occur, especially if a bone cement such as PMMA, is used to provide mechanical attachment to the device. The local rise in temperature that occurs when the monomer cross-links to form the polymer is

sufficient to kill bone cells to a depth of nearly a millimetre [38]. Some examples of prosthesis that require the use of PMMA are given in Figure 9 [39].

Figure 9: Examples of prosthesis for THA fixed with PMMA [38]

Stress shielding is also a major problem that occurs when the implant prevents the bone from being properly loaded. Since the implant has a higher modulus of elasticity, it carries almost all the load. The elastic modulus of cortical bone ranges between 7-25 GPa, depending on age, location of the bone and direction of measurement (bone is anisotropic). This modulus is 10 to 50 times lower than that of alumina (380 GPa). Cancellous bone has a modulus of elasticity that is several hundreds of times smaller than that of alumina.

Bone must be loaded in tension to remain healthy. Stress shielding weakens the bone in the region where the applied load is lowest or in compression. Bone that is unloaded or that is loaded in compression will undergo a biological change that leads to bone resorption.

The interface between a stress shielded bone and an implant deteriorates as the bone is weakened, resulting in loosening and or fracture of the bone. The presence of wear debris that often occurs in artificial hip and knee joints accelerates the weakening of the stress-shielded bone, because the increased cellular activity involved in removal of the foreign wear particles also attacks and destroys bone.

The combination of stress shielding, wear debris and motion at the interface is especially destructive and usually leads to failure [38].

4.2. Biomaterials for hip joint replacement

The average load in the hip joint is approximately three times the body weight. In addition, hip bones are subjected to cyclic loading as high as 10^6 cycles per year. Therefore, bone implants must have appropriate mechanical properties, close to bone. Metals, ceramics, polymers and composites have been investigated for use as biomaterials [40].

The hip joint consists of two complementary articular surfaces separated by articular cartilage and the synovial fluid with pH=7.29-7.45. The hip replacement has a cup type and a long femoral type element.

Metals have good mechanical properties, but exhibit poor biocompatibility, causing stress shielding and release of dangerous metal ions causing eventual failure or removal of implant. Titanium alloys and stainless steel show higher wear rates as compared to ceramics and cobalt-chromium alloys. Stainless steel matching polyethylene produce higher wear rates than cobalt-chromium on polyethylene [41].

Ceramics generally have good biocompatibility (causing reduced osteolysis), but poor fracture toughness and tend to fracture. Alumina possesses high strength, good biocompatibility and stability in physiological environments, being largely used for this application. But it presents lack of chemical bonding to the bone and therefore is not fitted for potential bone substitute. Due to alumina ability to be polished to a high surface finish and its excellent wear resistance, is often used for wear surfaces in joint replacement prosthesis, in the femoral heads. The alumina femoral head is used in combination with a metallic femoral stem and an acetabular cup made of UHMWPE.

Table 6 resumes some of the properties of ceramics used in Total Hip Replacement (THR) [40].

Composite materials usually present a combination of biocompatibility, mechanical strength and toughness, being object of growing interest.

In THR, the components are usually fit in place by cement, as referred before. Loosening of the components often happens at the interface between the cement and the bone. The bone cement (PMMA) interface is highly dynamic with degradation of the polymer in the cement and bone ingrowth [40].

Table 6: Mechanical properties of ceramics used in THR [40]

Ceramic	Compressive strength (MPa)	Tensile strength (MPa)	Elastic Modulus (GPa)
Zirconia	2000	820	220
Alumina	4000	300	380
Bioglass	1000		75
C – Graphite	138		25
C – Vitreous	172		31
HAP	600	50	117
C – LTI pyrolitic	900		28
AW glass-ceramic	1080		118

4.3. Wear mechanisms in hip implants

The implanted prosthesis requires revision within 10 years, and the life span of an implant is approximately 15 years. The factors that influence wear rates are:

- type of materials;
- contact stresses;
- surface hardness and roughness;
- type of articulation due to motion;
- number of cycles, solution particle count and distribution;
- oxidation of materials;
- surface abrasion of metal and polyethylene particulates [41].

Based on clinical studies, loosening and failure in THR are associated with osteolysis and bone resorption that are induced by polyethylene particles. These particles seem to be of approximately 1 μm size and often particulate or fibrous in shape [42]. Figure 10 shows a UHMWPE cup with advanced wear and the body response to the wear debris.

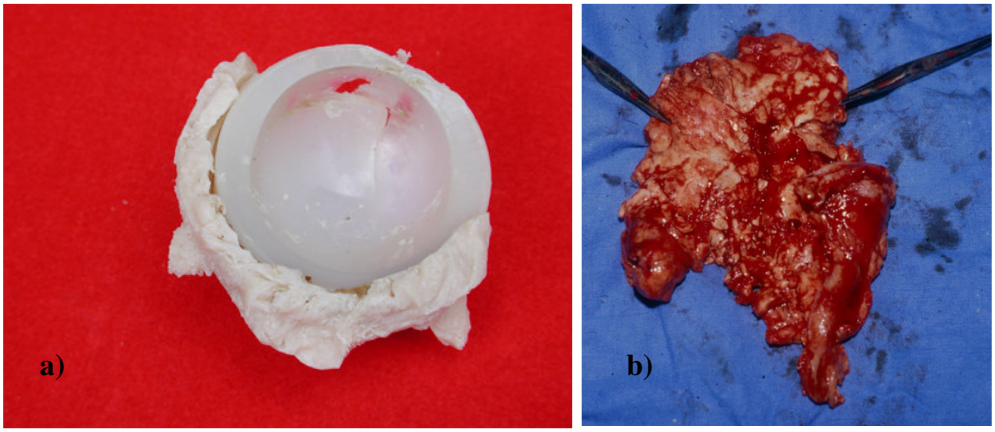

Figure 10: Wear of UHMWPE (a) and consequent foreign-body response in the synovial fluid (b) [39]

Osteolysis and aseptic loosening are the main causes for THR failure [43]. In this field of science there is a consensus that polyethylene such be eliminated in THR and substituted for ceramics in order to reduce the wear rate and eliminate the problem of osteolysis and consequent surgery [44].

Alternatives to polyethylene are [44]:

- improving the properties of hard metals, such as CoCrMo alloys;
- using hard coatings, such as diamond-like carbon, DLC, or coatings of the system Ti-Nb-N-O, such as TiN;
- improving the properties of oxide ceramics, such as single phase alumina or zirconia;
- using non-oxide ceramics, such as SiC or Si_3N_4.

4.4. Physiological response

The physiological response to a foreign body is a process that involves many immunogenic processes. The basic components of the immune response are leukocytes.

The immune response is divided into innate immunity and adaptive immunity.

The innate immunity is responsible for the initial defence against foreign particles. Its components are physical and chemical barriers, blood proteins, cytokines and phagocytic cells, like neutrophils and macrophages. Cytokines are cellular proteins that mediate inflammation and communication between cells of the immune system.

The adaptive immunity is controlled by lymphocytes and takes place after exposure to a foreign body.

When a wear particle is released from the implant surfaces into the synovial joint cavity, a macrophage engulfs the particle, loses is normal surface topography and displays a part of it on its surface, turning into an antigen presenting cell (APC).

A result of the inflammatory reaction is bone resorption, which is the process of breaking down bone. This is a natural process that usually takes place in the body, along with bone formation to replace bones. But excessive resorption leads to osteolysis and failure of the prosthesis. Cytokines have a major role in bone resorption stimulated by osteoclasts.

The size and morphology of debris is relevant because particles must have a critical size (0.1 – 10 μm) to cause macrophages to activate cytokines [44].

5. The bone

Bone can be defined as a dynamic and connective tissue, constituted by metabolically active cells that are included in a rigid framework [45].

The main functions of the bone in the maintenance of body systems are: protection of the vital organs, offer site and support of muscle attachment and locomotion, creation of red and white blood cells for immunoprotecion and oxygenation of other tissues and retention and storage of important ions such as calcium, phosphate and others [46].

5.1. Bone biochemistry

There are organic and inorganic elements in bone composition. The bone as 20% (weight) of water. The major component in weight of the dry bone is inorganic calcium phosphate (65-70%) and an inorganic matrix of collagen and fibrous proteins (30-35%).

The osteoblasts secrete the osteoid, which is the unmineralized organic matrix. It is mostly composed of type I collagen (90%) and 10% ground substance (noncollageneous proteins, glycoproteins, proteoglycans, peptides, carbohydrates and lipids) [45]. The collagen fibres are responsible for the elasticity and flexibility and organization of the matrix of the bone [47]. Bone's strength and rigidity is provided by the mineralization of

osteoid by inorganic mineral salts. Bone possesses a large amount of cations and complex anion groups, mostly Ca^{2+}, PO_4^{3-}, CO_3^{2-}. Other ions as Mg^{2+}, Fe^{2+} (in the blood), F^- and Cl^- are also present, but in smaller amounts. Calcium and phosphate ions originate the formation of calcium triphosphate and hydroxyapatite, present in the amorphous mineral fraction that is diffused and dispersed in the organic fraction. The mineral fraction is mostly constituted of hydroxyapatite [48].

5.2. Bone physiology

In an adult skeleton two types of bone can be found: the cortical (or compact) bone (80%) and cancellous (or trabecular) bone (20%) [46]. A primary type can be considered: the woven bone. This bone can be found during embryonic development, fracture healing (callus formation) and in some pathological states (hyperparathyroidism and Paget disease, for example). This bone is normally replaced with cortical or cancellous bone [45].

Considering the location in the skeleton, the proportion between the cortical and the trabecular bone varies. Trabecular bone is porous (50-90%), and therefore the modulus of elasticity and compressive strength is approximately ten times smaller than that of cortical bone, that is almost solid (10% of porosity). Trabecular bone possesses a "sponge-like" morphology, with a network of honeycombed interstices that contain plates, bars and rods of several sizes called trabeculae. Cortical bone, having low porosity, only possesses spaces for osteocytes, *canaliculi* and blood vessels [46]. A schematic representation of trabecular and compact bone is given in Figure 11.

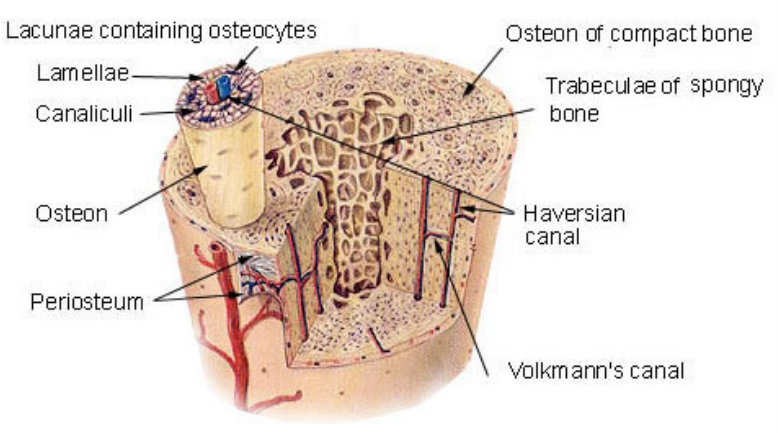

Figure 11: Schematic representation of the trabecular and compact bone [49]

The long bones are divided in three physiologic sections. The tubular shaft is denominated diaphysis. In the center of this section is the medullary cavity, filled in with marrow. At the end of each bone is the epiphysis, between the physis (growth plate) and the bone. The epiphysis is covered with cartilage. In the transition between the wide part of the bone and the tubular section is the diaphysis [46].

The cancellous bone can be found mostly in the metaphysis, and the cortical bone comprises the diaphysis, but sometimes the cortical bone forms a layer over cancellous bone aiming to improve the mechanical properties. Surrounding the cortical and cancellous bone there is a sheath called periosteum that is almost continuous, except near joints. It has two layers: an outer and fibrous layer, that connects bones to the joint, and an inner vascularized layer that contains cells capable of becoming osteoblasts. Periosteum has two important roles: fundamental for endochondral bone formation and make available a significant fraction of the bone's blood supply during life. The medullary cavity, Havers and Volkmanm channels (play the role of containers for the biggest blood vessels), and the cavities of cancellous bone are lined with a thin membrane called endosteum [46,50], as shown in Figure 12.

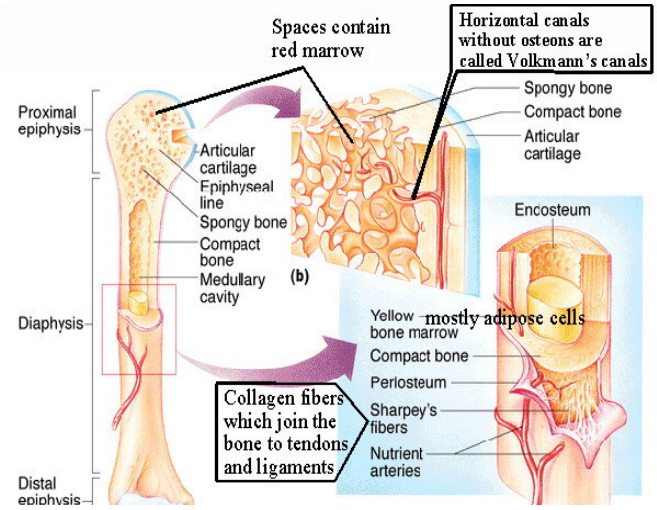

Figure 12: Scheme representing the physiological sections of a long bone [51]

The long bones and their marrow play an important role as storage containers of micronutrients as calcium and phosphorus (bone), as well as iron (marrow) [48].

The bone marrow is divided in red and yellow marrow. The red marrow is a myeloid (blood producing) tissue, responsible for the production of red and white blood cells. Red bone marrow fills the cancellous epiphysis of long bones. With age, it is largely replaced by yellow marrow for fat storage. In adults, red marrow is limited to the spongy bone in the skull, ribs, sternum, clavicles, vertebrae and pelvis. Red marrow functions in the formation of red blood cells, white blood cells and blood platelets. Yellow marrow consists mostly in fat cells. It can revert to red marrow under extreme hematopoietic stress, such as in blood loss [52-54].

5.3. Bone cells

Bone has the following cellular components: osteogenic precursor cells, osteoblasts, osteoclasts, osteocytes and the hematopoietic elements of bone marrow.[51]

The osteoblasts are bone cells of mesenchymal origin, that segregate unmineralized bone matrix (osteoid) that can eventually mineralize to yield mature bone, providing bone's strength and rigidity [45,48,54]. They are localized mainly in the *periosteum* membrane and in the endosteal membrane. At the end of their activity, osteoblasts imprisoned in their osteoid cell inside the bone matrix are converted to osteocytes.

Morphologically, osteoblastic cells are categorized in a linear sequence processing from osteoprogenitors to pre-osteoblasts to osteoblasts and finally to osteocytes and elongated (lining) cells [45].

Mature (terminally differentiated) osteoblasts that are trapped within the bone matrix, and are responsible for its maintenance (synthesize and resorb matrix to limited extend). Each osteocyte fills a space, the *lacunae*, and communicate with each other and with blood vessels through cylindrical *canaliculi*, filled with cytoplasmatic projections.

They are also responsible for the control of the extracellular concentration of phosphorous and calcium, providing a rapid release of these ions from mineralized bone into the blood [45,48,54].

The osteoclasts are multinucleated cells are responsible for bone resorption, controlled by hormonal and cellular mechanisms. They have a hematopoietic origin and resorb bone through secretion of acid and proteases [45,54].

The osteogenic precursor cells are present in all nonresorptive bone surfaces, as the deepest layer of the *periosteum*, in the *endosteum* and in the bone marrow [45].

5.4. Bone formation and remodelling

Intramembranous, endrochondral and appositional formation are the three processes responsible for bone formation. Intramembranous bone formation produces a woven or lamellar structure depending on the rate of apposition. Intramembranous bone formation produces primarily cortical bone present in the face, cranium, sternum and scapula.

Endrochondral bone formation occurs in embryogenesis and begins when mesenchymal stem cells start to differentiate into chondrocytes and secrete a cartilaginous matrix. Near the end of this part of the process MSCs begin to differentiate into osteoblasts that proliferate and form a bone matrix on the calcified cartilage.

The appositional formation occurs during enlargement of bones and during remodelling. The three types of formation occur continuously and a particular bone can be formed through the combination of these developmental processes [46].

Bone remodelling is a dynamic process that takes place all life long and is particularly intense in the period of somatic growth, due to the activity of osteoclasts and osteoblasts on the macroscopic periosteal and endosteal surface of bones. Its primary purpose is to adjust the bone mass to the mechanical stresses that the various skeleton parts undergo on average (skeletal homoeostasis) [48]. Bone remodelling has five distinct phases: resting state, activation, resorption, reversal and formation [46].

5.5. Bone healing

Fracture healing restores the tissue to its original physical and mechanical properties and it is influenced by a variety of systemic and local factors. Healing occurs in three stages: the early inflammatory stage, the repair stage and the late remodelling stage.

In the inflammatory stage there is the development of a hematoma in the fracture site (caused by bone fracture or implant placement) during the first few hours and days.

During the repair stage, fibroblasts begin to lay down a stroma that helps support vascular ingrowth. Parallel to this, a collagen matrix is deposited while osteoid is secreted

and mineralized, leading to the formation of a callus around the repair site. Ultimately, the callus ossifies, forming a bridge of woven bone between the fracture fragments.

During the remodelling stage the healing bone is restored to its original shape, structure and mechanical strength. This stage takes months or years and can be facilitated by mechanical stress placed in the bone. As the fracture site is exposed to an axial loading force, bone is laid down where is needed and resorbed from where it is not needed [45].

6. Biocompatibility evaluation

Biocompatibility can be defined as the ability of a man made material to exist in an *in vivo* environment for an acceptable period of time, with no detrimental effect to the host. Material properties that are relevant to biocompatibility include chemical inertness, toxicity, thrombogenicity and resistance to adhesion [55].

Biomaterials must be evaluated to determine if they are biocompatible and will have an appropriate behaviour in the *in vivo* environment.

Cell adhesion, proliferation and differentiation

Cell adhesion is involved in several natural phenomena like embryogenesis, maintenance of tissue structure, wound healing, immune response, metastasis as well as tissue integration of the biomaterial [56]

In a first phase, it occurs the cell attachment to the biomaterial, adhesion and spreading. The success of this first phase influences the cell's capacity to proliferate and to differentiate in contact with the implant [56]. Moreover, the behaviour and functioning of adherent cells (shape, proliferation, and synthetic function) depend on the characteristics of the substrate, specially its adhesiveness [57].

The attachment phase occurs rapidly, involving short-term events like physico-chemical linkages between cells and materials involving several types of forces (ionic, van der Walls, etc), and the adhesion phase that involves numerous biological molecules: extracellular matrix proteins, cell membrane proteins and cytoskeleton proteins. The more cells spread, the higher is their rate of proliferation. For differentiation to occur is

necessary a high cell density, enhanced cell-cell interactions and cell-matrix interactions in the presence of several differentiation factors [57].

Cell culture methods – in vitro studies

To perform cell culture experiments, cells are removed from original organs or tissues and placed in an artificial environment, where, using a specific medium that provides the necessary nutrients for survival and growth is maintained for a desired period of time.

A toxic material is a material that releases a chemical in sufficient quantities to kill cells directly or indirectly through inhibition of key metabolic pathways. Many factors influence the toxicity of a chemical (compound, temperature, test system, etc.) being the dose or amount of chemical delivered to the individual cell the most important factor [58].

The main objective of the toxicity testing is to develop an adequate database to make reasonable and reliable judgements concerning the safe use of biomaterials in the human body. For toxicological *in vitro* studies, isolated cells are the most widely used systems, including freshly isolated cells in suspension, primary cell cultures, cell lines, cell strains and cocultures. The advantages of the use of *in vitro* systems in toxicity assessment using cells are [59]:

- improved efficiency, reduced cost;
- reduction in the use of experimental animals;
- greater control over nature of cell population;
- direct control over extracellular medium, chemical concentration, duration of exposure;
- freedom from potential confounding factors such as hormones, nervous system or immunity;
- replicates are available from same stock

But they also present some disadvantages such as the loss of in vivo organ morphology, selected loss of *in vivo* organ-specific functions, loss of possible mitigating

influences, such as hormones, nervous system or immunity, generally a static system resulting in progressive loss of nutrients and accumulation of metabolic end products [59].

Finite or continuous cell line

Primary cultures are the most chosen system, mostly because they retain their original capabilities and properties to a greater extent in isolation, simulating the *in vivo* response more closely. Cocultures perform even better in this point, but require a greater effort in optimizing the conditions that replicate the *in vivo* response [60].

After several subcultures a cell line will die (*finite cell line*) or alter to become a *continuous cell line* that has the ability to grow continuously. Continuous cell lines can also be obtained from tumour tissues. The advantages of continuous cell lines are their greater growth rates to higher cell densities, their lower serum requirement and general ease of maintenance in simple media and their ability to grow in suspension. The disadvantages are, among others, the greater chromosomal instability, divergence from the donor phenotype and loss of tissue-specific markers.

Almost all culture cells are propagated as a monolayer, anchored to a glass or plastic substrate, but in some cases, like transformed cells, haemopoietic cells and ascites tumours, can be *propagated in suspension*. This has the advantage of simpler propagation (subculture only requires dilution, no trypsinization) and the possibility of achieving a "steady-state" culture if required [60].

Assay Methods

Three primary cell culture assays are used for evaluating biocompatibility: direct contact, agar diffusion and elution (or extract dilution). These assays are morphological ones, meaning that the outcome is measured by observations in the morphology of the cells. They vary from each other in the way that the test material is exposed to the cells.

The test material may be placed directly on the cells or extracted in an appropriate solution that is then placed on the cells. Positive or negative controls are usually included in the assays to guarantee the operation and suitability of the test system. The negative control is often a high-density polyethylene material [58].

References Chapter I

[1] Bourrat X., Structure in Carbon and Carbon Artifacts. In Marsh H., Reinoso F.R. editors, Sciences of Carbon Materials, Publicaciones Universidad de Alicante, 2000

[2] Pierson H., Handbook of carbon, graphite, Diamond and Fullerenes – Properties, Processing and Applications, Noyes Publications, 1993

[3] Reich S., Thomsen C., , Phil. Trans. R. Soc. Lond. A (2004) 362, 2271-2288

[4] Grill A., Meyerson B.S., Development and Status of Diamondlike Carbon. In Spear H.E., Dismuhes J.P. editors, Synthetic Diamond – Emerging CVD Science and Technology, Wiley-Interscience, John Wiley and Sons, Inc., 1994

[5] Robertson J., Materials Science and Engineering R 37 (2002) 129-281

[6] Zhang S., Bui X.L., Jiang J., Xiaomin L., Surface and Coatings Technology 198 (2005) 206 - 211

[7] Lettington A.H., Carbon 36 (1998) 555-560

[8] Cui F.Z., Li D.J., Surface and Coatings Technology 131 (2000) 481-487

[9] Butter R., Allen M., Chandra L., Lettington A.H., Rushton N., Diamond and Related Materials 4 (1995) 857-861

[10] Allen M., Myer B., Rushton N., In J. Biomed. Mater. Res. (Appl Biomater) 58: 319-328, 2001

[11] Narayan R.J., Materials Science and Engineering C 25 (2005) 405-416

[12] Dearnley G., Arps J.H., Surface and Coatings Technology 200 (2005) 2518-2524

[13] Dowling D.P., Kola P.V., Donnely K., Kelly T.C., Brumitt K., Lloyd L., Eloy R., Therin M., Weill N., Diamond and Related Materials 6 (1997) 390-393

[14] Ohring M., The Materials Science of Thin Films, Academic Press Inc., 1992

[15] Albella J.M, Deposición por Pulverización Catódica., In. Abella J.M. Laminas delgadas: preparación e aplicaciones, Consejo Superior de Investigaciones Científicas, 2002

[16] Kelly P.J., Arnell R.D., Vacuum 56 (2000) 159-172

[17] Arnell R.D., Kelly P.J., Surface and Coatings Technology 112 (1999) 170-176

[18] Arnell R.D., Kelly P.J., Surface and Coatings Technology 188-189 (2004) 158-163

[19] Zhang S., Bui X.L., Yongquig F., Surface and Coatings Technology 167 (2003) 137-142

[20] Logothetidis S., Gioti S., Materials Science and Engineering B46 (1997) 119-123

[21] Chowdhury S., Laugier M.T., Rahman I.Z., Journal of Materials Processing Technology 153-154 (2004) 804-810

[22] Andújar J.L, Pino F.J., Polo M.C., Pinyol A., Corbella C., Bertran E., Diamond and Related Materials 11 (2002) 1005-1009

[23] Hill D., Design Engineering of Biomaterials for Medical Devices, John Wiley & Sons, 1998

[24] Dressler W., Riedel R., Int. J. of Refractory Metals & Hard Materials 15 (1997) 13-47

[25] Petzow G., Herrmann M., Silicon Nitride Ceramics, Structure and Bonding, Vol. 102, Springer-Verlag Berlin Heidelberg 2002

[26] Besson J.L., Rouxel T., Goursat P., Scripta Materialia Vol. 39, No. 10, pp. 1339-1343, 1998

[27] Wiederhorn S.M., Hockey B.J., French J.D., Journal of the American Ceramic Society 19 (1999) 2273-2284

[28] Takadoum J., Houmid-Bennani H., Mairey D., Journal of the European Ceramic Society 18 (1999) 553-556

[29] Rosenflanz A., Current Opinion in Solid State and Materials Science 4 (1999) 453-459

[30] Hench L.L., Wilson J., Introduction. In Hench L.L., Wilson J, editors, An Introduction to Bioceramics, Advanced Series in Ceramics – Vol. 1, World Scientific, 1993

[31] Hench L., Best S., Ceramics, Glasses and Glass-ceramics. In Ratner B, Hoffman A., Schoen F., Lemons J. editors, Biomaterials Science – An Introduction to Materials in Medicine, Second Edition, Elsevier Academic Press, 2004

[32] Adapted from www.madehow.com/Volume-5/Bioceramics.html

[33] Salgado J.A:, Coutinho O.P., Reis R.L., J. Biomed. Mater. Res. 44 (1999) 98-108

[34] Hölland W., Beall G., Glass-Ceramic Technology, The American Ceramic Society, 2002, pp. 145-146

[35] Ravaglioli A., Krajewski A., Bioceramics: Materials, Properties, Applications, Chapman & Hall, 1992

[36] Hallab N.J., Jacobs J.J., Katz L., Orthopedic Applications. In Ratner B, Hoffman A., Schoen F., Lemons J. editors, Biomaterials Science – An Introduction to Materials in Medicine, Second Edition, Elsevier Academic Press, 2004

[37] Ambrosio L., Peluso G., Davis P.A., Biomaterials and their Biocompatibilities. In Wise D.L., Trantolo D.J., Altobelli D.E., Yaszemski M.J., Gresser J.D. editors, Human Biomaterials Applications, Humana Press, 1996

[38] Hench L.L., Wilson J., Introduction. In Hench L.L., Wilson J, editors, An Introduction to Bioceramics, Advanced Series in Ceramics – Vol. 1, World Scientific, 1993

[39] Notes from the Discipline of "Prosthesis, Implants and Artificial Organs", First year of the Masters Degree

[40] Katti K. S., Colloids and Surfaces B: Biointerfaces 39 (2004) 133-142

[41] Buford A., Goswami T., Materials and Design 25 (2004) 385-393

[42] Wang A., Sun D.C., Stark C., Dumbleton J.H., , Wear 181-183 (1995) 241-249

[43] Sargeant A., Goswani T., Materials and design 27 (2006) 287-307

[44] Willmann G., Advanced Engineering Materials 3 (2001) No. 3

[45] Kalfas I.H., Neurosurg Focus 10 (4): Article 1, 2001

[46] Vassilios I.S., Johnna S., Temenoff S., Mikos A.G., Biomaterials 22 (2001) 2581-2593

[47] Boskey A.L., Mineralization, structure an function of bone. In: Seibel M.J., Robins S.P., Bilezikian J.P., Dynamics of Bone and Cartilage Metabolism, Academic Press, 1999

[48] Ravaglioli A., Krajewski A., Bioceramics – Materials, Properties, Applications, Chapman & Hall, 1992, pp. 17, 21-26

[49] Adapted from www.web-books.com/.../skeletal/skeletal.htm

[50] Locke M., Journal of Morphology 262: 546-565 (2004)

[51] Adapted from www.unm.edu/~jimmy/skeletal_notes.htm

[52] Majumdar M.K., Thiede M.A., Mosca J.D., Moorman M., Gerson S.L., Journal of Cellular Physiology 176:57-66 (1998)

[53] Bianco P., Riminucci M., Gronthos S., Gehron Robey P., Stem Cells (2001) 19; 180-192

[54] Le Blanc K., Tammik L., Sundberg B., Haynesworth S.E., Ringdén O., Scandinavian Journal of Immunology 57 (2003) 11-20

[55] Robling A.G., Castillo A.B., Turner C.H., Annu. Rev.Biomed. Eng. 2006.8:455-498

[56] Anselme K., Biomaterials 21 (2000) 667-681

[57] Schoen F.J., Mitchell R.N., Tissues, the Extracellular Matrix and Cell-Biomaterial Interactions. In Ratner B, Hoffman A., Schoen F., Lemons J. editors, Biomaterials Science – An Introduction to Materials in Medicine, Second Edition, Elsevier Academic Press, 2004

[58] Northup S.J., In Vitro Assessment of Tissue Compatibility. In Ratner B, Hoffman A., Schoen F., Lemons J. editors, Biomaterials Science – An Introduction to Materials in Medicine, Second Edition, Elsevier Academic Press, 2004

[59] Tyson C.A., Stacey N.H., In Vitro technology, Trends and Issues. In In Vitro toxicity Testing – Applications to Safety Evaluation, Frazier J.M.editor, Marcel Dekker, Inc., 1992

[60] Freshney R.I., Introduction to basic principles. In Animal Cell Culture, Second Edition, Freshney R.I. editor, IRL Press, 1992

Chapter II

In Vitro assessment of DLC

(Adapted from "Biocompatibility evaluation of DLC-coated Si_3N_4 substrates for biomedical applications", E. Salgueiredo, M. Vila, M.A. Silva, M.A. Lopes, J.D. Santos, F.M. Costa, R.F. Silva, P.S. Gomes, M.H. Fernandes, submitted to Diamond and Related Materials, April 2007)

1. Introduction

Some medical applications require materials with a non cell-adhesive surface, such as devices in contact with human blood (e.g., artificial heart valves), while others need a cell-adhesive surface to assure complete tissue integration of the implanted material in the human body. In orthopaedic applications, the osteointegration is promoted by the formation of an apatite layer on the surface of the biomaterial upon implantation. The biomaterial surface properties can be defined aiming to control its bioactivity and biocompatibility. For applications such as replacement of the hip joint, which is composed of a stem, a femoral head and an acetabulum, the formation of an apatite layer is desired on the stem, but not at femur head or acetabulum surface since it would compromise the tribo-system performance. There are many different shapes, sizes, and designs of artificial components of the hip joint, made of several materials such as chrome, cobalt, titanium, polymeric or ceramic materials. Nevertheless, on going problems with wear and particulate debris still exist, causing metallosis, and eventually periprosthetic osteolysis and aseptic loosening [1].

Si_3N_4 based ceramics are well known for their superior combination of fracture toughness and hardness [2]. These are key properties for an excellent wear resistance, which, combined with Si_3N_4 chemical inertness, turns this material a suitable candidate for high-load medical applications, namely for metal prostheses replacement. In order to diminish the friction forces in such kind of bio-tribological systems, the Si_3N_4 surfaces must be modified. DLC coatings are of enormous interest for biomedical applications due to their biocompatible, auto-lubricious, and non-stick properties [3-5]. Therefore, DLC is a very good candidate for coating the hip joint tribosystem, especially when combined with the adequate bio-mechanical properties of the Si_3N_4 ceramic [6].

Surface properties such as surface chemistry, surface energy and surface topography can be critical for biomaterials biocompatibility, together with bulk properties characteristics. Protein adsorption, which is a virtually instantaneous process during an implantation procedure, is a dynamic and a very complex phenomenon that precedes any cell-mediated effects either *in vitro* or *in vivo*. Biomaterial surface properties, important in protein adsorption, that can be readily quantified, include interfacial free energy, hydrophobicity and surface charge density.

2. Experimental

2.1. Silicon nitride processing

The first stage of this work was the processing of dense silicon nitride based ceramics. The mixture was prepared using commercial powders: α-Si_3N_4 (Starck grade C), Y_2O_3 (Starck grade M11) and Al_2O_3 (ALCOA CT-3000SG) in an 89.3 / 7.0 / 3.7% weight proportion, respectively. The mixed powders were Si_3N_4 ball milled (Retsch PM 400) for 8h in a isopropyl alcohol media and the homogeneous suspension was dried at 60 ºC and sieved with an 100 μm mesh.

After consolidation of the powder by uniaxial pressing at 30 MPa, the substrates were isostatic pressed at 200 MPa and then placed in a graphite crucible covered by a powder bed of Si_3N_4/BN (1:1). The sintering was performed in a graphite furnace (Thermal Technologies Inc.) at 1750 ºC for 2h in a nitrogen atmosphere. The sintering cycle is schematically described in Figure 1.

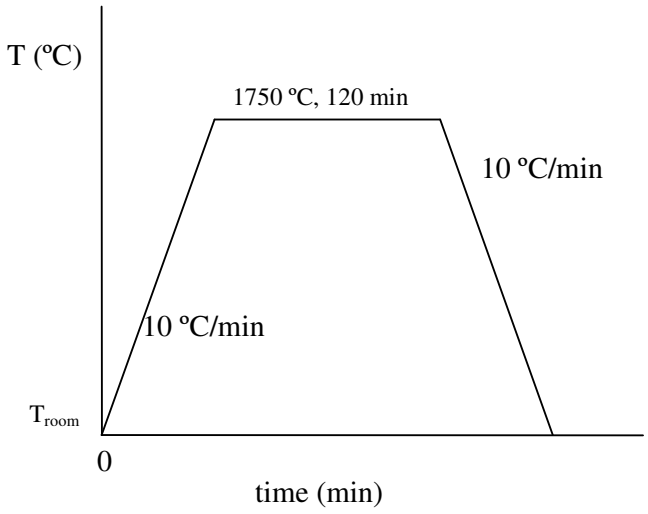

Figure 1: Thermal cycle for the sintering of the Si_3N_4 based ceramics

The density of a sample can be determined by the immersion method, in which the body is immerged in a liquid with a known density.The density of the sintered samples was measured using the Archimedes equation:

$$d = \frac{w_{dry}}{w_{dry} - w_{wet}} \times d_e \qquad \text{(Eq. 1)}$$

Were:

d – density (g/cm^3)

W_{dry} – weight of the sample in the balance

W_{wet} – weight of the immersed sample

d_e – density of etilenoglycol, $C_2H_6O_2$ (1,11 g/cm^3)

The samples were weighted in a digital balance (A&D instruments Lda, GR-200-EC), with a 0.0001g resolution. The densification of the substrates was evaluated by the following equation:

$$\rho = \frac{d}{d_t} \times 100\,\% \qquad \text{(Eq. 2)}$$

ρ being the density of the samples, d_t the theoretical density (3,2540 g.cm^{-3}) of the powders mixture (α-Si_3N_4, Y_2O_3 and Al_2O_3) and d the calculated density of the samples by the Archimedes Method. By this procedure, fully dense (>99% of theoretical density) substrates were obtained.

The substrates were ground to obtain the same final disc-shaped dimensions (10 mm in diameter and 3 mm in thickness).

Before the deposition of the DLC films, the substrates surface was polished in order to evaluate the effect of the surface roughness in the adhesion of the DLC film to the substrate, according to the following steps:

i. Ground polishing with a 15 μm diamond slurry (Diamit, Industrial Diamond), in an automatic polishing machine (Kemet 15) over a cast iron plate;
ii. Polishing with a 15 μm diamond slurry in an automatic polishing machine (200rpm) (Metaserv 200) over a 15 μm diamond cloth;
iii. Polishing with a 6 μm diamond slurry in an automatic polishing machine (200rpm) (Metaserv 200) over a 6 μm diamond cloth;
iv. Cloth polishing with colloidal silica, 0.25 μm (SBT, South Bay Technologies).

2.2. DLC sputtering

The DLC deposition was carried out using a planar 3'' magnetron sputtering source operated by a DC power supply (CRIOLAB PC 30.1) with a rotary pump and a turbomolecular pump (ALCATEL ATP 400).

Figure 2: DC magnetron sputtering used in this work (Physics Dep., University of Aveiro).

A study of the deposition parameters of the a-C/DLC coatings over Si_3N_4 based ceramics on the DC magnetron sputtering apparatus was performed, to obtain the optimized values that combined good adhesion, low intrinsic stress and high hardness, as briefly resumed in Tables 1 and 2.

Initially, Si_3N_4 substrates with different polished surfaces (15 μm and 6 μm diamond slurry and colloidal silica (0.25 μm)) were used to evaluate the combination between roughness and adhesion. The lowest substrate roughness was obtained with the colloidal silica finishing, but good adhesion in this ultra-polished surfaces was harder to obtain.

In the beginning of the optimization of the deposition parameters, a study of the current intensity was performed, starting with low intensity values. By increasing the intensity there was an increase in the deposition rate, with similar coating morphology.

But, for current intensities higher than 0.40 A an overheating of the graphite target occurred, compromising the safety of the procedure. Therefore, the current intensity value was set in the range 0.30-0.40 A.

Table 1: Study of the current intensity, I

Sample	**DC Power (kW)**	**V (V)**	**Ar flow (sccm)**	**Residual Pressure, P_{res} (mbar)**	**Working Gas Pressure, P_w (mbar)**	**Time (min)**	**I (A)**
A1	0.30	365	72	~ 10^{-5}	5x10^{-3}	30	0.09
A2		388					0.19
A3		392					0.30
A4		404					0.40

After establishing an adequate range for the current intensity, an evaluation of the optimal working gas pressure, P_w, was conducted. After several experiments the optimized pressure was established for 10^{-3} mbar.

The deposition time was also studied (results not shown). DLC coatings possess a major drawback which is the high internal stress in the as-deposited coatings. As the deposition time increases aiming to obtain thicker films, the higher is the internal stress, leading to the formation of blisters and consequent delamination of the film.

Table 2: Study of the Working Gas Pressure, P_w at constant current Intensity

Sample	**DC Power (kW)**	**V (V)**	**I (A)**	**Ar flow (sccm)**	**Time (min)**	**Residual Pressure, P_{res} (mbar)**	**Working Gas Pressure, P_w (mbar)**
B1	0.15	501	0.30	25	30	4*10^{-6}	1*10^{-3}
B2	0.16	529		18		4*10^{-6}	~ 10^{-4}
B3	0.13	466		100		~ 10^{-5}	10^{-2}
C1	0.20	501	0.40	72		5*10^{-6}	10^{-3}

The optimized parameters for DLC deposition on Si_3N_4 substrates are those indicated for sample C1. These parameters combine good adhesion, high deposition rate and excellent microstructural properties.

Before deposition of the amorphous carbon, an intermediate layer of Si was deposited by the same technique from a silicon wafer target, in order to promote adhesion between the Si_3N_4 substrates and the DLC films, for further tribological tests.

2.3. Surface measurements and *in vitro* assays

Zeta potential measurements were performed in Anton Paar EKA- Electro Kinetic Analyser equipment, using a rectangular cell in which the solution passes along a channel formed by two layers of the sample separated by an inert spacer. AgCl electrodes at each end of the channel were used to determine the potential generated by the flow. The measurements were performed using 0.001 M KCl as electrolyte solution, at pH 7.4 ± 0.2. The zeta potential, ζ, is calculated from:

$$\zeta = (V_S/\Delta p)\times(\eta/\varepsilon\varepsilon_0) \times(L/A)\times(1/R) \quad \text{(Eq. 3)}$$

where V_S is the streaming potential, Δp the hydrodynamic pressure difference across the sample, η is the viscosity and ε the permittivity of the liquid, ε_0 the permittivity of free space, L and A are the length and cross sectional area of the sample and R is the electrical resistance across it. Fairbrother and Mastin's [7] approach was used to determine the term L/A.

For surface tension and contact angle determinations, water, glycerol and diiodomethane (Merk Schuchardt, > 99%) were the test liquids. Water was distilled and deionised, while diiodomethane was doubly distilled under vacuum. Contact angles were measured on the DLC coated surfaces using the sessile drop technique in a video-base system DATA Physics Contact Angle System OCA 15. The drop is deposited directly on the surface of the material from a micrometric syringe with a metallic needle.

The ellipse method was used to fit a mathematical function (Laplace-Young Fitting) to the measure drop contour line. For each experiment, were analysed no less than

12 drops. The measurements were carried out at 25 ºC inside a refrigerated stainless steel chamber, with glass windows of optical quality and saturated with the liquid in analysis.

Young's equation establishes the contact angle of a liquid drop resting on a solid surface, θ, from the relation between the surface tension of a liquid in equilibrium with its vapour, γ_{LV}, the solid-vapour surface tension, γ_{SV}, and the solid-liquid interfacial tension, γ_{SL} : $\gamma_{LV} \cos \theta = \gamma_{SV} - \gamma_{SL}$. The Owen and Wendt's approach [8] postulates that the total surface tension can be expressed as the sum of the dispersive, γ^d, and the polar, γ^p, components. The solid-liquid interfacial tension can be rewritten as:

$$\gamma_{SL} = \gamma_{SV} + \gamma_{LV} - 2\sqrt{\left(\gamma_{SV}^{d}\,\gamma_{LV}^{d}\right)} - 2\sqrt{\left(\gamma_{SV}^{p} - \gamma_{LV}^{p}\right)} \qquad \text{(Eq. 4)}$$

Using Young's equation and Equation 4, γ_{SV} and γ_{SL} can be determined taking the values of contact angles measured with some testing liquids whose surface tension components are known.

A simulated body fluid (SBF) solution was prepared as reported in literature [9] for *in vitro* testing, by dissolving reagent-grade NaCl, $NaHCO_3$, KCl, $K_2HPO_4.3H2O$, $MgCl_2.6H2O$, $CaCl_2$ and Na_2SO_4 into deionised water, and buffered at pH 7.40 with tris(hydroxymethyl)amminomethane ($(CH_2OH)_3CNH_3$) and hydrochloric acid (HCl) at 37 ºC. Triplicate samples were soaked into SBF solution in sterile polystyrene bottles for 7, 21 and 35 days. A ratio of solution volume to surface area of the specimen was kept at 0.1 ml/mm^2. After soaking, samples were analyzed using SEM to detect apatite layer formation, and changes in ionic concentrations were evaluated by inductive plasma coupled atomic emission spectrometry (ICP-AES). Changes in the pH of the fluid were also registered.

MG63 osteoblast-like cells were cultured in α-Minimal Essential Medium containing 10% fetal bovine serum, 50 μgml^{-1} ascorbic acid, 50 μgml^{-1} gentamicin and 2.5 μgml^{-1} fungizone, at 37ºC in a humidified atmosphere of 5% CO_2 in air. For subculture, adherent cells were enzymatically released (0.05% trypsin, 0.25% EDTA) and cultured (10^4 $cellcm^{-2}$) for 3 days in control conditions (absence of materials, standard polystyrene tissue culture plates) and on the DLC coated Si_3N_4 material surface. Control cultures and seeded DLC films were evaluated for cell adhesion and morphology (SEM) and cell

viability/proliferation (MTT assay). For SEM observation, samples were fixed with 1.5% glutaraldehyde in 0.14 M sodium cacodylate buffer (pH 7.3), dehydrated in graded alcohols, critical-point dried, sputter-coated with gold and analysed in a JEOL JSM 6301F scanning electron microscope. Cultures were observed at 1, 5, 24 and 72 hours.

In the MTT assay, cultures were incubated with 0.5 $mgml^{-1}$ of MTT (3-[4,5-dimethylthiazol-2-yl]–2,5-diphenyltetrasodium bromide) during the last 4h of the culture periods tested (24 and 72 hours); the medium was then decanted, formazan salts were dissolved with 200 μL of dimethylsulphoxide and the absorbance was measured at 600 nm in an ELISA reader. The results were normalized in terms of macroscopic area and expressed as Acm^{-2}.

2.3. Results and Discussion

Figure 3 shows the surface of DLC coated Si_3N_4 samples before (a) and after 35 days of immersion in SBF solution (b), as observed by SEM. No apatite layer or any other type of deposits can be seen on these ultra-high smooth surfaces. Also, ICP measurements showed no significant changes on the ionic concentration levels of calcium, phosphorous, magnesium and sodium with immersion time.

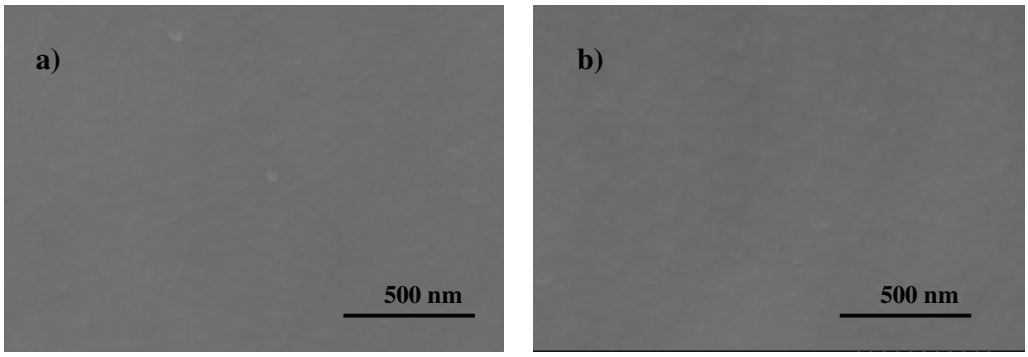

Figure 3: Surface of DLC coated Si_3N_4 samples before (a) and after 35 days of immersion in SBF solution (b), as observed by SEM.

The DLC coated surface is only slightly negative charged, as denoted by the zeta potential value of -35.0±1.3mV at pH 7.4±0.2, which explains the low Ca^{2+} ions adsorption that would be imperative for further nucleation of an amorphous apatite layer.

The surface tension of DLC coated samples was found to be 45.7mN/m (Table 3). The dispersive component of the surface tension is predominant (36.6mN/m), corresponding to a contribution of about 80% to the total surface tension.

Values in Table 3 were calculated from the measurements of contact angles on DLC (65.8º ± 5.8º for water; 55.4º ± 4.7º for glycerol; and 40.9º ± 3.8º for diiodomethane), which are in the range of the values published in the literature, obtained for samples coated with DLC by other methods [10].

Table 3: Surface tension of testing liquids [10] and the values determined for the DLC coated Si_3N_4 biomaterial

	Surface Tension (mN/m)	**Dispersive component, (mN/m)**	**Polar component, (mN/m)**
Water	71.5	21.4	50.1
Glycerol	63.4	37.0	26.4
Diiodomethane	50.5	50.5	0
DLC coatings	45.7	36.6	9.1

MG63 osteoblast-like cells were used for a quick screening biocompatibility assay of the prepared DLC coated Si_3N_4 samples.

After cell plating, few cells were able to attach to DLC films, as evident in Fig. 4a, showing the appearance of the surface at 1 h. After 24 h, adherent cells presented a normal morphology (Fig. 4b). Neighbouring cells have connection with each other through cytoplasmic extensions and proliferated with culture time (Figs 4b and c).

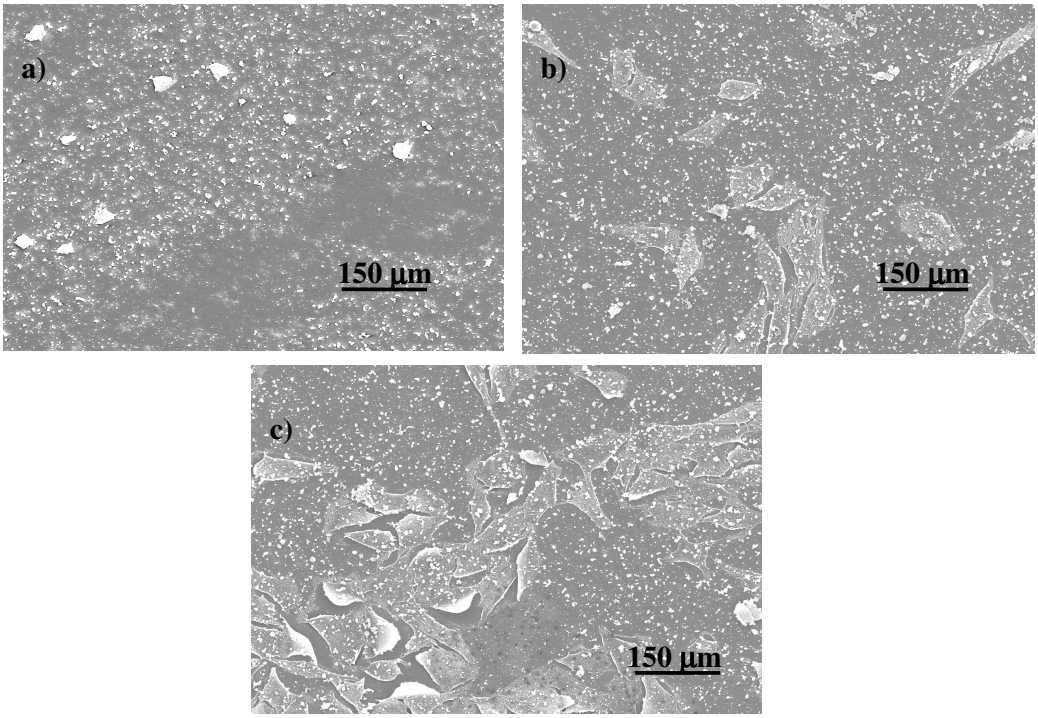

Figure 4: Surface of DLC coated Si_3N_4 samples seeded with MG63 osteoblastic-like cells. SEM appearance at 1 h (a), 24 h (b) and 72 h (c)

As compared to control cultures (performed in standard polystyrene tissue culture plates), MTT reduction was very low at 24 h, but results at 72 h showed that cell growth rate was significantly higher on the seeded DLC surface, as shown in Figure 5.

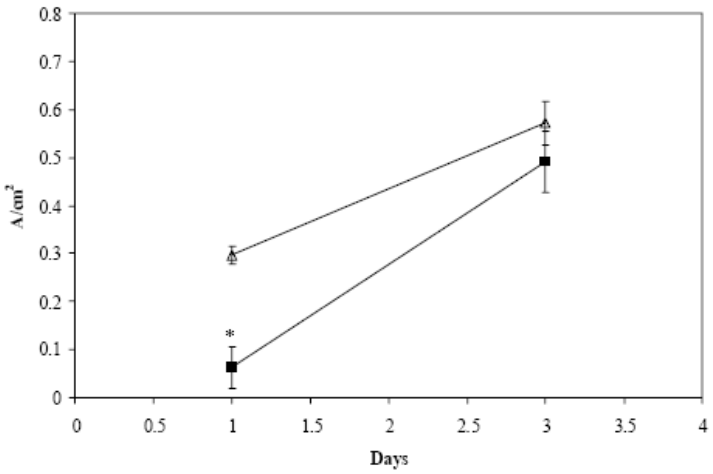

Figure 5: Cell viability/proliferation. Control (▲) and DLC surface (■).*Significantly different from control

It is well known that surface charge, along with wettability, plays an important role in the biological response to implant materials and, despite the widely varied observations reported in the literature, some generalizations may be made from *in vitro* published studies [11]. Given that virtually all interfaces are charged in aqueous solution, and that biomolecules carry a net charge, it is intuitive that electrostatic interactions will play a role in the cell response. Moderately hydrophilic surfaces appear to induce more favourable cell responses than hydrophobic materials, by favouring adsorption of proteins and better preserving their bioactivity. Both positively- and negatively-charged surfaces are able to bind adhesion proteins and support cell adhesion. However, the mode of cell adhesion is distinct for positive and negative charges, since cell membranes, that carry a negative charge, adhere very closely to positively charged surfaces, whereas contact occurs only at distinct points on near-neutral and negatively charged surfaces [12-14]. These differences can be attributed primarily to electrostatic attraction and repulsion, respectively, but also demonstrated quantitative and qualitative patterns in protein adsorption and functionality.

The results of the present work regarding the interaction of MG63 osteoblastic cells with the DLC coated Si_3N_4 material during the first 24 h do not suggest an optimum surface for cell adhesion. Although with an optimized experimental design favouring the cell adhesion process (plating of a cell suspension over a plane surface), only few cells were able to attach to the DLC films, as evident by SEM observation and also from the MTT reduction values measured at 24 h. The negative value of ZP of the surface may have contributed, in synergy with its wettability properties, to the poor cell adhesion observed. However, it is worth to mention that attached cells presented a normal pattern of cell spreading displaying the typical morphology at 24 h without no evidence of cytotoxicity. In addition, compared to the cell behaviour observed in standard polystyrene culture plates, the DLC adherent cells showed a significantly higher cell growth rate, as suggested by the MTT assay.

These observations are in line with previous biocompatibility studies performed in several cell culture systems, namely mouse peritoneal macrophages, mouse fibroblasts, murine macrophage cell line IC-21, human synovial fibroblasts, osteoblast-like SaOS-2 cells and glial and fibroblast cell lines with no indication of cytotoxicity in vitro and cell growth kinetics studies reporting that cells generally grew faster on DLC [15, for a

review]. These properties render DLC-coated Si_3N_4 attractive to be used as femoral head and the acetabulum hip joint components, in which cell adhesion is not desirable.

2.4. Conclusions

The excellent set of intrinsic characteristics of Si_3N_4 (bioinertness, low density, high fracture toughness) ceramics can be further improved by adherent, biocompatible, DLC coatings, regarding hip replacement medical applications. The DLC films are slightly negative surface charged, exhibiting a zeta potential of -35.0±1.3mV.

The total surface tension is 45.7mN/m, with a minor polar component (9.1mN/m), which turns the DLC coating quite hydrophobic. As a result of this, DLC showed no apatite layer formation ability in vitro testing using an acellular simulated body fluid (SBF).

Also, no evidence of cytotoxicity was demonstrated by cells normal morphology and higher cell growth rate compared to standard culture plates, although with low cell adhesion. These properties render DLC-coated Si_3N_4 attractive to be used as femoral head and the acetabulum hip joint components, in which cell adhesion is not desirable.

References Chapter II

[1] Sargeant A., Goswami T., Materials and Design 27 (2006) 287.

[2] Petzow G., Herrmann M., In: Janson M. (Ed.), High Performance Non-Oxide Ceramics II, Structure and Bonding V. 102, Springer-Verlag, Berlin, 2002, p. 47.

[3] Narayan R.J., Mater. Sci. Eng. C 25 (2005) 405.

[4] Cui F.Z., Li D.J., Surf. Coat. Techn. 131 (2000) 481.

[5] Zhao Q., Liu Y., Abel E.W., J. Colloid Interface Sci. 280 (2004) 174.

[6] Vila M., Abreu C.S., Salgueiredo E., Almeida F.A., Fernandes A.J.S., Costa F.M., Gomes J.R., Silva R.F., Thin Solid Films 515 (2006) 2192.

[7] Fairbrother F., Mastin H., J. Chem. Soc. 75 (1924) 2318.

[8] Owens D.K., Wendt R.D., J. Appl. Polym. Sci., 13 (1969) 1741.

[9] Kokubo T., Takadama H., Biomaterials 27 (2006) 2907.

[10] Strom G., Fredriksson M., Stenius P., J. Colloid Interface Sci 119 (1987) 352.

[11] Schulz H., Leonhardt M., Scheibe H.J., Schultrich B., Surf. Coat. Techn. 200 (2005) 1123.

[12] Wilson C.J., Tissue Engineering 11 (2005) 1.

[13] Haynes C.A., Norde W., Colloids Surf. B: Biointerfaces 2 (1994) 517.

[14] Davies J.E., Causton B., Bovell Y., Davy K., Sturt C.S., Biomaterials 7 (1986) 231.

[15] Dearnaley G., Arps J.H., Surf. Coat. Techn. 200 (2005) 2518.

Chapter III

Tribological behaviour of DLC coatings

(Adapted from "Reciprocating sliding behaviour of self-mated a-C/DLC coatings on Si_3N_4 ceramics under tribological stress", M. Vila, C.S. Abreu, E. Salgueiredo, F.A. Almeida, A.J.S. Fernandes, F.M. Costa, J.R. Gomes, R.F.Silva, Thin Solid Films 515 (2006) 2192-2196

and

"Bio-tribological performance of a DLC-UHMWPE system", M. Vila, C.S. Abreu, I.Ochando, E. Salgueiredo, F.M. Costa, J.R. Gomes, R.F. Silva, submitted to Surface and Coatings Technology, June 2007)

1. Introduction

Biotribology can be defined as the science of tribology applied to functional biological systems, particularly considering the synovial joints and their artificial replacement. It's related to the articulation of natural and artificial bearing systems under applied loads and motions, and, being a discipline of tribology, involves the related areas of friction, wear and lubrication.

The main feature that determines the characteristic of bearing, at a microscopic level, is whether or not the prevailing conditions can maintain full fluid film lubrication thus preventing the contact between the two articulating surfaces. In this situation, the load is supported by the fluid between the bearing surfaces, which results in the reduction of the frictional resistance and wear. But, when contact between the two surfaces occurs, there is an increase in friction and in the amount of generated wear debris, which can originate an unfavourable response from the host system [1].

DLC films are notable for their combination of very low friction coefficients and high wear resistance, justifying its widespread usage in tribological applications such as protective coatings for magnetic storage devices, car parts, biomedical devices, and on novel micro- and nanoscale electromechanical devices (MEMS, NEMS) [2-4].

Many distinct metallic/non-metallic substrate materials have been used for the deposition of DLC films. A general requirement for high-load mechanical applications is that the substrate/film system is made of materials presenting a low hardness and bulk modulus mismatch in order to avoid coating failure. Silicon nitride is a hard, tough and chemically inert material. Due to its physical and chemical properties, Si_3N_4 finds applications in several fields, mostly those dealing with tribo-mechanical uses in harsh environments. Nonetheless, the Si_3N_4 tribological performance can be improved by coating it with a wear resistant low friction coefficient material, such as the carbon based hard films. Silicon nitride based ceramics have been successfully coated with micro and nano crystalline diamond by CVD [5] ensuring good adhesion levels, for future mechanical applications.

Therefore, this material fulfils the pre-requisites to be a substrate for DLC deposition. Tribologically, amorphous carbon (a-C), one of the various forms of DLC [2], performs better than hydrogenated amorphous carbon films in moderate/high humidity environments and aqueous lubricated sliding such as those found in many biomedical

applications [6]. Although the friction and wear behaviour of DLC films has been studied by several authors, information regarding the specific tribological performance of self-mated DLC in ambient atmosphere is scarce in the open literature [7]. Self mated sliding experiments are adequate to assess the intrinsic tribological properties of hard materials as well as the behaviour of emergent tribosystems, e.g. MEMS, NEMS and mechanical seals [8,9].

Friction, wear and consequent loosening of wear debris are one of the reasons of prosthesis failure. Loosen particles provoke the reaction of the organism by treating them as foreign bodies, creating inflammations and possible necrosis of the nearest tissues [10-12]. These processes end up with the release of prostheses components till the necessity of substituting the device by performing an aggressive operation to the patient [13].

Most of the total joint prostheses (e.g. hip, knee and temporomandibular) are metallic made parts of alloys such as Ti6Al4V, CoCr and CoCrMo, or ceramic materials (Al_2O_3, ZrO_2) [14], that work against Ultrahigh Molecular Weight Polyethylene (UHMWPE) components. Both metallic and polymeric wear debris activate macrophages and may provoke loss of bone tissue [15].

In order to avoid these problems, the substitution of the metallic part by an inert ceramic body coated with an autolubricant and protective coating is here proposed. The development of new tribomaterials for mechanical bearing applications, avoiding the use of pollutant lubricant oils, has favoured the search for solid lubricant coatings. Carbon coatings such as diamond-like carbon (DLC) have been extensively studied due to their low coefficient of friction against several materials, coming from a grafitic tribolayer action. The good tribological performance of DLC and its proven biocompatibility opened the window for other tribo-applications like synovial joint prosthesis [16]. The use of a bioinert ceramic material for DLC substrate, such as silicon nitride (Si_3N_4), assures the biocompatibility [17].

The tribological behaviour of DLC/UHMWPE systems has been reported in literature, but only related to DLC coated metallic parts. Hip simulators testing demonstrated the UHMWPE wear reduction against DLC coated stainless steel, CoCr and Ti6Al4V heads in comparison to uncoated parts, reporting UHMWPE wear rate values in the 10^{-6} mm^3/Nm range [18-20]. Also, a similar beneficial effect of DLC coating of CoCr for knee joint applications was demonstrated by a five times reduction of UHMWPE wear

comparing to uncoated control materials [21]. Vacuum arc deposited DLC over Ti6Al4V were tested against UHMWPE in pin-on-disc configuration in water lubricated conditions leading to the reduction of the friction coefficient from 0.07 without coating to 0.02 for multilayer DLC coatings, although with local to severe coating damage, depending on the film structure [22]. Platon et al. [23] carried out an extensive work on the tribological characterization of DLC coated Ti6Al4V and 316L stainless steel by plasma enhanced CVD against UHMWPE in dry conditions, reporting friction coefficients of about 0.2 and DLC wear rates in the range 10^{-5} mm^3/Nm. For a more detailed description, recent overviews on DLC coated parts for biotribological purposes can be found in the literature [24,25]

Even though the extensive work on DLC coatings for orthopedic implants, failures by delamination in clinical tests still happened [26]. Adhesion improvement is thus an additional reason for the present proposal of coating silicon nitride (Si_3N_4) ceramics with DLC together with avoiding of metallosis disease. Primary tribological characterization of dissimilar Si_3N_4-DLC coated/UHMWPE pairs was carried out by dry sliding experiments. Subsequently, *in vitro* tribological behaviour was assessed in simulated body fluid (SBF) environment. To overcome the adhesion problem typical of the DLC films due to residual stresses, interlayers or graded compositions of TiN, TiCN and TiC are normally used in the case of deposition over Ti alloys. In this work, a silicon interlayer over Si_3N_4 was used with the same purpose as its effectiveness has been already tested in other mechanical DLC applications [27].

2. Self-mating experiments

2.1. Experimental

In this work, Si_3N_4 and Si_3N_4/TiN composite substrates were sputter coated with a-C/DLC films in order to evaluate the tribological performance of self-mated pairs using a reciprocal dry sliding arrangement.

Two ceramic substrate types were synthesised: Si_3N_4 and a Si_3N_4/TiN composite. Both ceramic compositions were densified by pressureless sintering at a dwell temperature of 1750 ºC for 2h, in the case of the Si_3N_4 and 5h for the Si_3N_4/TiN composite, always

under a N_2 pressure of 0.1 MPa. After sintering, the dense ceramics were cloth polished in colloidal silica after polishing in 15 µm diamond slurry.

The a-C/DLC films were grown on Ø 10 mm x 3 mm disc shaped samples using a 3 inch planar magnetron sputtering source operated by a DC power supply with substrate bias capability. A circular graphite target with a thickness of 3 mm was clamped to the water cooled electrode. The Si_3N_4 balls were heated up to 200ºC during deposition for adhesion enhancement. The vacuum system provided a residual pressure near $1x10^{-6}$ mbar. The DC power was ~ 200W with Ar as the sputtering gas, while the used bias voltage was -175 V.

The tribological testing of self-mated a-C/DLC films was made on a reciprocating sliding tribometer (PLINT TE67/R), shown in Figure 1.

Figure 1: Tribometer with a ball-on-flat geometry (Mechanics Dep., University of Minho, Guimarães)

The oscillating arrangement consisted on a ball-on-flat geometry. The experiments were conducted in ambient atmosphere (~ 50-60% R.H.), under unlubricated conditions, with a constant stroke of 6 mm and frequency of 1 Hz. Sliding distances were varied in 25-86 m range. By means of dead weights, static applied normal loads of 3 N and 5 N were applied, which corresponds to an estimated mean Hertzian pressure (normal stress) of

~ 0.97 GPa and ~ 1.04 GPa, respectively [28]. The friction signal was acquired by means of a load cell, calibrated by applying external dead-weights in the range of the applied normal loads.

The microstructural morphology and topography of the as deposited and worn samples were characterized by scanning electron microscopy (SEM) and atomic force microscopy (AFM) in tapping mode. The predominant wear mechanisms were also identified.

2.2. Results and discussion

Silicon nitride substrates sputtered with an a-C/DLC coating without bias application revealed low adhesion, as confirmed by the plot of Fig. 2, which represents the friction coefficient evolution with the sliding distance.

The steep increase of the friction coefficient after ~3 m of sliding distance under an applied load of 5 N in the reciprocating test corresponds to adhesion failure.

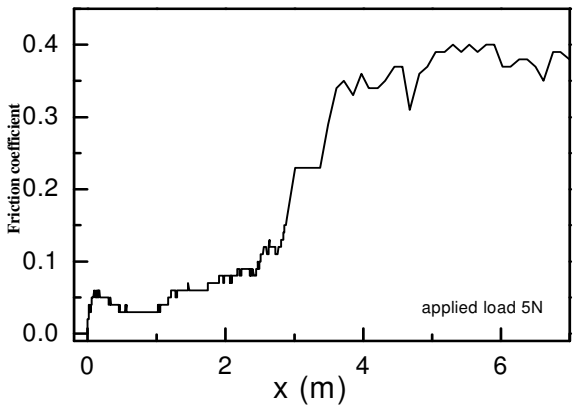

Figure 2: Friction coefficient vs. sliding distance corresponding to unbiased a-C/DLC film grown on Si_3N_4 substrate, showing adhesion failure after ~3 m

The delamination phenomena extended to the all wear track region, as depicted in Figure 3a). A detail of the wear track edge, Figure 3b), clearly evidences the well defined boundary between the film and the exposed substrate.

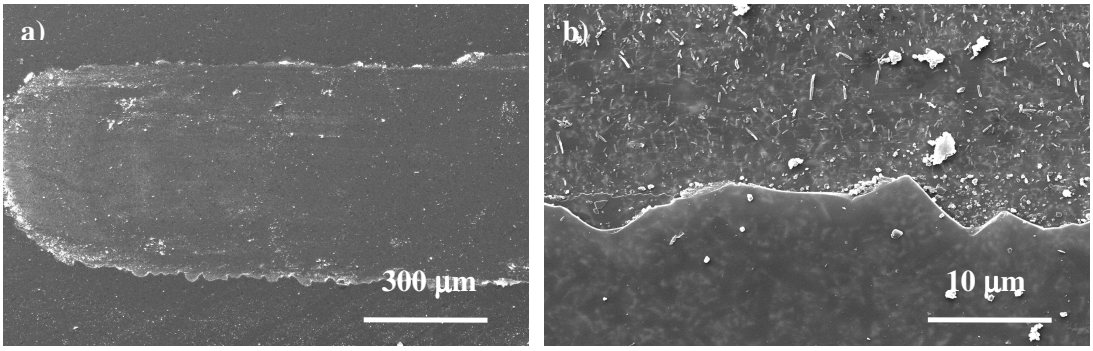

Figure 3: (a) low magnification SEM micrograph of the wear track region, denoting extensive film delamination; (b) detail of the margin of the same wear track evidencing a well defined film contour.

As an attempt to overcome the adhesion problem, a DC substrate bias voltage was applied during film deposition, resulting however in insufficient enhancement of the tribological behaviour. The insulating nature of the Si_3N_4 substrate compromised the bias effectiveness that proved to be essential for the tribological performance improvement of a-C/DLC films. Consequently, it was necessary to modify the ceramic substrate composition in order to render it conductive. Therefore, new substrates were prepared by adding TiN to the ceramic composition thus obtaining a Si_3N_4/TiN composite, having close mechanical properties to those of the Si_3N_4. In fact, to a slight hardness reduction (15.5GPa to 14.9GPa) corresponded a small toughness increase (6MPa·$m^{-1/2}$ to 7.6MPa·$m^{-1/2}$).

This Si_3N_4/TiN composite material is suitable for electro-discharge machined EDM cutting tools [29]. Prior to deposition, the surface roughness was estimated on each substrate type from AFM measurements, showing similar rms values of ~ 6 nm and ~ 7 nm for the Si_3N_4 and the Si_3N_4/TiN composite, respectively. A slight increase on the surface roughness was found after the deposition of ~ 0.4 µm thick a-C/DLC films, the coating on Si_3N_4 presenting a value of ~ 8.7 nm and ~12 nm on the composite. Hence, the starting surface roughness conditions of the two coated substrate types for the tribological tests are similar.

Representative AFM scans of worn a-C/DLC surfaces deposited on the composite are shown in Fig. 2. A scan taken at the edge of the wear track, Fig. 4a, reveals a surface degradation induced by tribological stress on the track region (rms roughness ~ 97nm) in opposition to a smoother surface corresponding to the unworn a-C/DLC film. Inside the wear track, groves along the sliding direction are perceptible. This phenomenon is evidenced by the AFM image taken at the centre of the wear track, Fig. 4b.

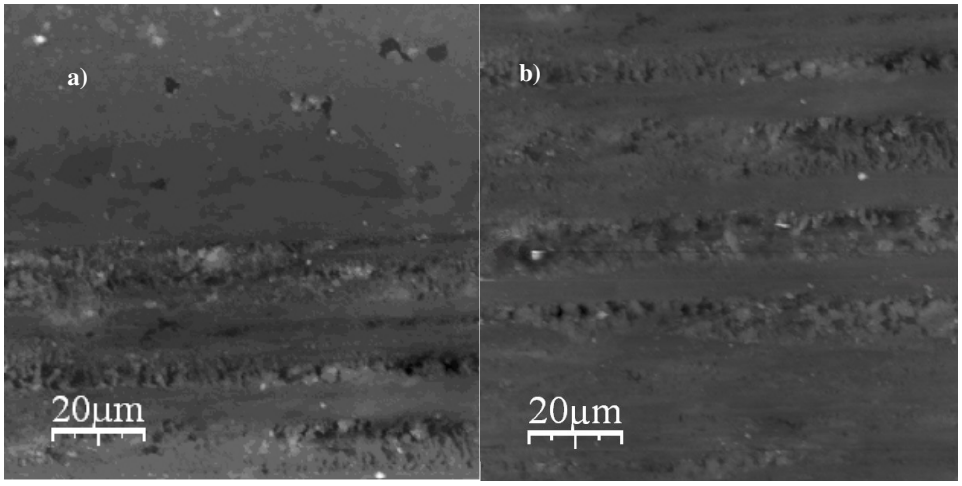

Figure 4: 3D AFM representations of (a) edge of the wear track, showing the transition from the smooth a-C/DLC coating to the hilly region inside the track and (b) the centre of the wear track showing grooves and a plateau formed by debris smearing.

In addition, lumps of material resulting from smeared a-C/DLC wear debris are found in some regions of the wear track, forming plateaus. The low magnification SEM image of the same wear track in Figure 5a) shows a well preserved a-C/DLC film after tribological interaction, in opposition to the above described behaviour of the Si_3N_4 unbiased sample, Figure 3a). The micrograph in Figure 5b) details a representative region inside the wear track formed after ~ 40 m of distance slid under a load of 3 N. As it can be seen, only small portions of film were detached and fragmented, leaving smeared residues in the vicinity of the spalled zone.

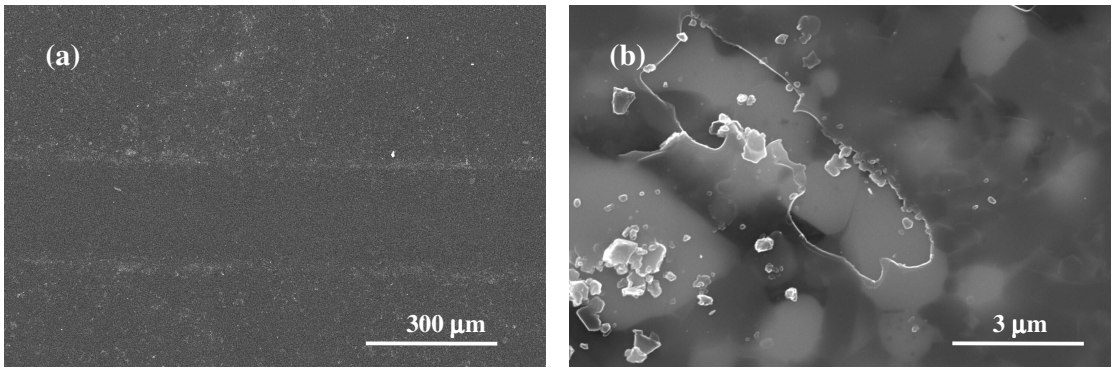

Figure 5: SEM micrographs of well preserved bias sputtered a-C/DLC film on the composite substrate in (a) low magnification and (b) detail, inside the wear track, evidencing sporadic film flaking

Typical friction coefficient evolution curves as a function of sliding distance are represented in Figure 6. In order to infer the influence of the applied load, sliding tests were performed at 3 N and 5 N for the same distance on coated Si_3N_4/TiN composite substrates.

For 3 N, Figure 6a), very low friction coefficient values of ~ 0.015 were attained after an initial transient regime of slightly higher values associated with the mechanical interaction of surface asperities. Friction coefficient values of this order were sustained for the full length of the sliding tests, ~ 43 m. Such weak frictional interaction between self-mated DLC pairs in ambient atmosphere can be explained by the transformation of the superficial layers in the contact zone into graphitic-like material, which act as a solid lubricant. Intercalation of water vapour between the graphitic layers led to low friction coefficients [28]. Such considerations find support in reported results by other authors concerning the friction behaviour of non-hydrogenated amorphous carbon coatings, which describe the aforementioned transformation of coating layers into graphitic material [2,30].

The Figure 6b) shows the results for the friction coefficient of the same tribosystem, subjected to a higher applied load, 5 N. As can be seen, the friction coefficient increases instantaneously to values of the order of ~ 0.25, which remain stable during the full duration of the test. These values are due to premature coating delamination on the ball specimen, which was later confirmed by the presence of exposed substrate, essentially resulting in the sliding contact of the dissimilar pair Si_3N_4-DLC.

In order to assess the influence of the negative bias voltage on the friction performance of the DLC films, similar sliding tests were made under an applied load of 3 N on an unbiased coated flat specimen, Figure 6c). In opposition to what is observed in Figure 6a) for a biased coated sample, the film on the ball failed immediately as the test started, revealing a distinct ball coating interaction with different DLC film types. The plotted curve reveals two distinct regions, the first one related to a premature ball coating failure, characterized by fairly stable moderate friction coefficient values in the 0.15-0.20 range. Once more, those values are associated to a Si_3N_4-DLC tribocontact, which persisted up to a sliding distance of ~ 15 m. The second region starts by an abrupt transition that indicates the coating failure, this time on the flat specimen. This corresponds to a more drastic sliding contact condition between two exposed Si_3N_4 based materials counter surfaces, which is characterized by high friction coefficient values in unlubricated

sliding [31]. The films on unbiased substrates failed by premature delamination even for the lowest loading condition (3 N, 0.97 GPa).

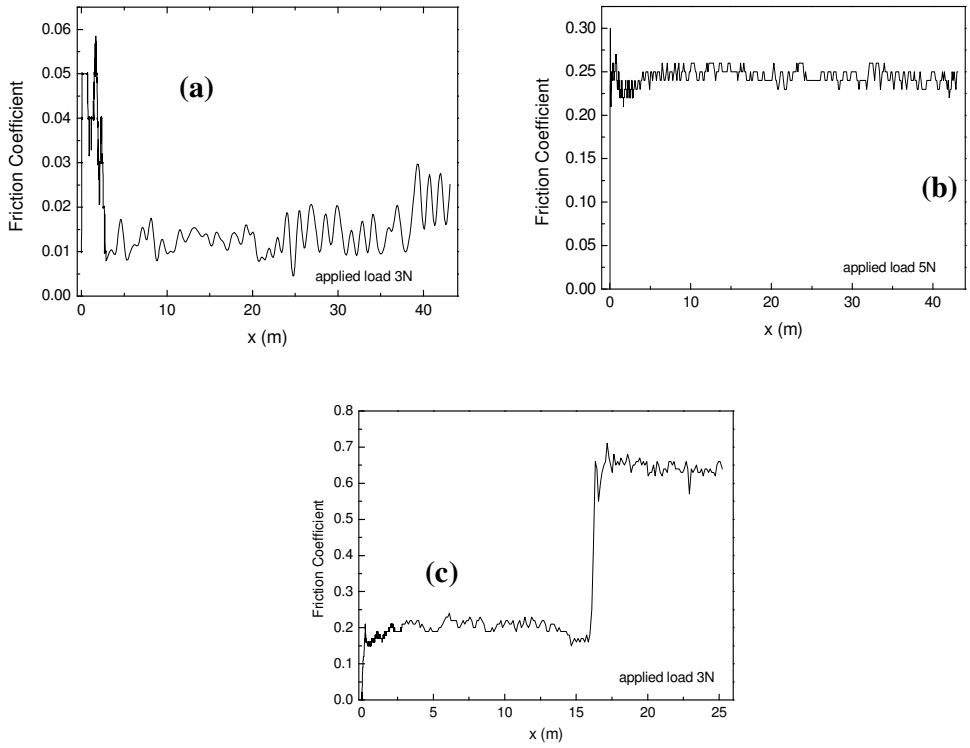

Figure 6: Representative friction coefficient evolution curves vs. sliding distance of DLC coated ball on a) bias sputtered composite flat specimen under 3 N, b) under 5 N, c) unbiased sputtered composite under 3 N.

2.3. Conclusions

Smooth a-C/DLC coatings were deposited by magnetron sputtering on Si_3N_4 based ceramic balls and discs for self-mated reciprocating dry sliding experiments. The films on unbiased substrates failed by premature delamination even for the lowest loading condition (3 N, 0.97 GPa). A remarkable improvement was achieved when the substrate composition was modified by adding 30% vol. of TiN, resulting in a conductive composite ceramic, allowing the effective application of a negative bias voltage.

Under the same tribological solicitation, very low friction coefficient values of ~ 0.015 were sustained during the full duration of the test (1 h, ~ 43 m). This behaviour assured unmeasurable wear, although the sliding track in the flat specimen suffered a

roughness increase from the nominal rms value of ~ 12 nm to ~ 97 nm, as a result of surface grooving and wear debris accumulation.

3. DLC/UHMWPE pairs

3.1. Experimental

Pressureless sintered silicon nitride ceramics were used in this work. Disc shaped (∅10 mm×3 mm) ceramic substrates were cloth polished in 6 μm diamond slurry, prior to DLC deposition. DLC films were deposited by d.c. magnetron sputtering from a 2" circular graphite target with a thickness of 3mm that was clamped to the water cooled electrode. A silicon interlayer was deposited by sputtering from a pure silicon target in-between the ceramic and the DLC coating to improve adhesion.

The tribological testing was made on a macro-scale tribometer (PLINT TE67/R) for high loads (20 N) and a micro-scale one (CETR UMT-2) for low loads (0.1 N). In both apparatus, the oscillating arrangement consisted on a ball-on-flat geometry. The ball-shaped parts were UHMWPE commercial (K-MAC Plastics) spheres (∅6 mm), while the flat specimens were the home-made DLC coated Si_3N_4 ceramic discs. The experiments were conducted under unlubricated conditions in ambient atmosphere (50–60% R.H.), and *in vitro* lubricated conditions.

A simulated body fluid (SBF) solution was prepared as reported in literature [32] for *in vitro* testing. Tests were performed with a constant stroke of 6 mm and frequency of 1 Hz for sliding distances of 690 m. By means of deadweight, static applied normal loads of 20 N and 0.1 N were applied, which correspond to estimated mean Hertzian pressures (normal stress) of 46 MPa and 7.9 MPa, respectively [33]. These calculations have taken into account the UHMWPE (0.69GPa) and Si_3N_4 (280GPa) Young's moduli, and Poisson coefficients of 0.3 and 0.46, respectively.

The counterparts morphology and the worn surfaces were characterized by field emission Scanning Electron Microscopy (SEM Hitachi S4100) and Atomic Force Microscopy (Digital Instrument Multimode IIa).

3.2. Results and discussion

Dense, smooth and well adhered DLC films were deposited with a thickness of approximately 500 nm and a surface roughness of R_a=11 nm over the Si_3N_4 discs. Its structural and mechanical characterization has been reported elsewhere, revealing a non-columnar growth with a significant sp^3 content leading to hardness and Young's modulus values of 16.3 and 156 GPa, respectively [34,35].

Preliminary dry tribological tests under 20 N during 16 h have been carried out in order to evaluate the performance of the DLC films under aggressive conditions and long periods. Film adhesion is here evaluated under an applied load that induces a nominal contact stress higher than that expected in real life.

As it can be seen in Figure 7, after a short initial "running-in" accommodation period, the coefficient of friction kept constant during the entire test with a value of 0.25. The ephemeral peak at the beginning of the tests is typical of dry sliding and corresponds to the surface asperities levelling-off. The present friction coefficient value is similar to the averaged one of dry friction DLC/UHMWPE experiments reported by Platon et al. [23], but the present friction curve is much more stable, free of fluctuations, even at higher contact pressures.

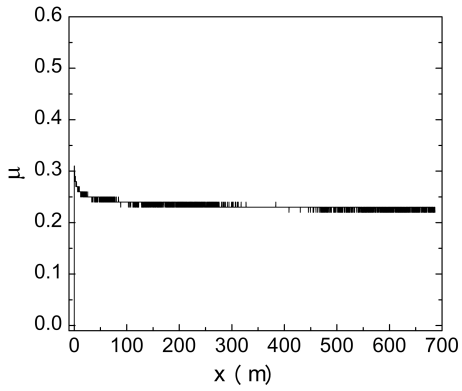

Figure 7: Friction coefficient curves from the tests of DLC coated discs against UHMWPE balls in unlubricated conditions and applied load of 20N

In order to visually inspect wear traces, SEM characterization was performed. The DLC coated ceramic specimens remain immaculate with no polymer transfers, Fig. 2a). No measurable wear in the UHMWPE ball could be assessed using conventional weight loss technique.

Measurements from near-circular wear scars imprinted on the ball were problematical because of the slight marks as it can be seen in Fig. 2b). The absence of any delamination events on the surface demonstrated the adequate adhesion of DLC on Si_3N_4 ceramic substrates. The absence of abrasive marks on both contact surfaces allows to infer adhesion as the main responsible friction mechanism for the moderate value of 0.25 of the friction coefficient. The adhesive wear mode of UHMWPE is known to come from the formation of a surface layer along the sliding direction induced by the disentanglement of the polymer chains [36].

After successfully testing in dry conditions, the DLC coatings were characterized by simulating the real working solicitation in articulated prostheses. Lubricated testes in SBF solution were carried out at a load of 0.1N, which corresponds for these materials and this geometry to an estimated mean Hertzian pressure of 7.9 MPa, as said before. This value is comparable to those present in articulated prosthesis, like the hip and knee joints, 3.45 and 6.90 MPa, respectively [37].

As it can be seen in Figure 8, the friction coefficient attained the value of 0.2 from which starts to decrease until the very low value of 0.02. The same value was found by Xu and Pruitt [22] for DLC coated Ti6Al4V sliding against UHMWPE in water.

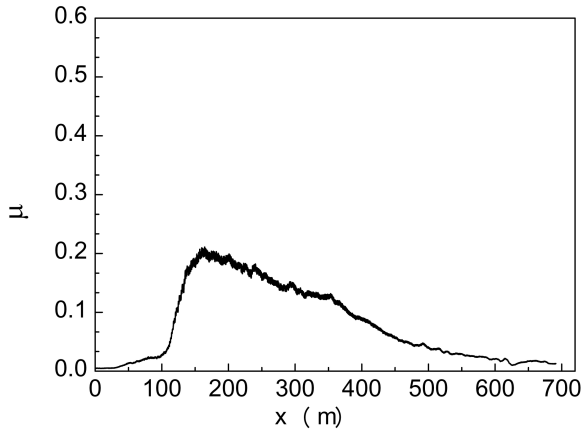

Figure 8: Friction coefficient curves from the tests of DLC coated discs against UHMWPE balls in SBF lubricated conditions and applied load of 0.1N

Contrarily to the results of the later study, the coated disc does not show any wear marks, Figure 9c), and neither does the UHMWPE ball, Figure 9d), meaning that wear is

unmeasurable. Also, the film did not present any signs of delamination and no transferred layers of polyethylene.

The relatively high initial friction values, similar to the dry friction coefficient, are probably related to a partial dry sliding contact before a complete liquid boundary layer is formed. It is worth noting that dry friction conditions occur in implanted hip prosthesis functioning during jumping, for example [23].

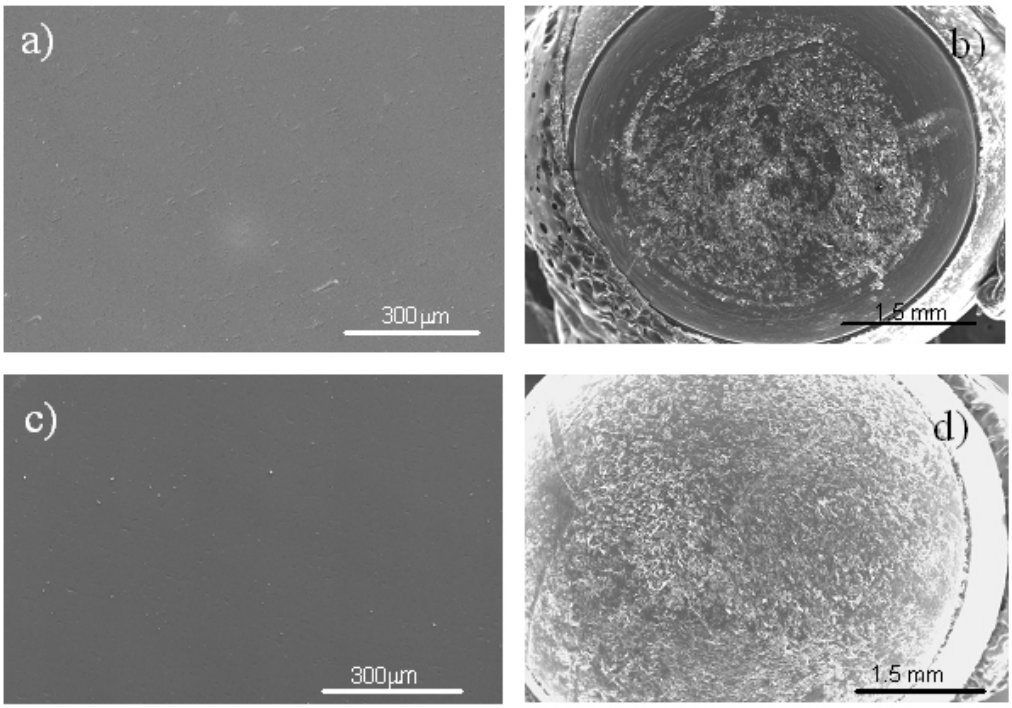

Figure 9: SEM pictures of DLC coatings (a,c) and UHMWPE surfaces (b,d) tested under unlubricated conditions and load of 20N (a,b) and SBF lubricated conditions and applied load of 0.1N (c,d).

This tribosystem denotes a superior performance in dry and simulated body fluid (SBF) lubricated conditions. The absence of any delamination events in both solicitations demonstrates the adequate adhesion of DLC on Si_3N_4 ceramic substrates. On the other side, no wear marks neither polymer transfers are present in the DLC coated surfaces which implies the protection of the opposite UHMWPE body, where wear scars are unmeasurable. In dry sliding conditions, adhesion is the main friction mechanism leading to a value of 0.25 for the friction coefficient, while the SBF lubrication diminishes this value to 0.02. The present results demonstrate that the coating of bioinert Si_3N_4 ceramics with DLC envisages a direct application in articulated joint prostheses.

3.3. Conclusions

For reciprocating sliding experiments against UHMWPE balls, Si_3N_4 ceramic discs were coated with DLC by magnetron sputtering. This tribosystem denotes a superior performance in dry and simulated body fluid (SBF) lubricated conditions. The absence of any delamination events in both solicitations demonstrates the adequate adhesion of DLC on Si_3N_4 ceramic substrates. On the other side, no wear marks neither polymer transfers are present in the DLC coated surfaces which implies the protection of the opposite UHMWPE body, where wear scars are unmeasurable.

In dry sliding conditions, adhesion is the main friction mechanism leading to a value of 0.25 for the friction coefficient, while the SBF lubrication diminishes this value to 0.02. The present results demonstrate that the coating of bioinert Si_3N_4 ceramics with DLC envisages a direct application in articulated joint prostheses.

.

References Chapter III

[1] Hall R.M., Bankes M.J.K., Blunn G., Current Orthopaedics (2001) 15, 281-290

[2] Robertson J., Mater. Sci. Eng. R 37 (2002) 129.

[3] Grill A., Surf. Coat. Technol. 94-95 (1997) 507.

[4] Goldsmith J., Sutter E., Moore J.J., Mishra B., Crowder M., Surf. Coat. Technol., in press.

[5] Abreu C.S., Oliveira F.J., Belmonte M., Fernandes A.J.S., Silva R.F., Gomes J.R., Wear 259 (2005) 771.

[6] Ronkainen H., Varjus S., Holmberg K., Wear 222 (1998) 120.

[7] Jia K., Li Y.Q., Fisher T.E., Gallois B., J. Mater. Res. 10 (6) (1995) 1403.

[8] Forbes S., Wilson J. I.B., Thin Solid Films 420-421 (2002) 508.

[9] Jones G.A., Wear 256 (2004) 433

[10] Voevodin A.A., Zabinski.S., Diam. Rel. Mater. 7 (1998) 463.

[11] Neerinck D., Persoone P., Sercu M., Goel A., Kester D., Bray D., Diam. Rel. Mater. 7 (1998) 468.

[12] Donnelly K., Dowling D.P., Connell M.L., Flood R.V., Diam. Rel. Mater, 3(1999) 538.

[13] Grill A., Diam. Rel. Mater. 8 (1999) 428.

[14] Willmann G., Adv. Eng. Mater. 3 (2001) 135.

[15] Kurtz S.M.; Muratoglu O.K., Evans M., Edidin A.A., Biomaterials 20 (1999) 1659.

[16] Erdemir A., Donnet C., J. Phys. D: Appl. Phys. 39 (2006)311.

[17] Kue R., Sohrabi A., Nagle D., Frondoza C., Hungerford D., Biomaterials 20 (1999) 1195.

[18] Saikko V., Ahlroos T., Calonius O., Keränen J., Biomaterials 22 (2001) 1507.

[19] Dowling D.P., Kola P.V., Donnelly K., Kelly T.C., Brumitt K., Lloyd L., Eloy R., Therin M., Weill N., Diam. Rel.Mater. 6 (1997) 390.

[20] Affatato S., Frigo M., Toni A., J. Biomed. Mater. Res. 53 (2000) 221.

[21] Oñate J.I., Comin M., Braceras I., Garcia A., Alava J.I., Surf. Coat. Technol. 142-144 (2001) 1056.

[22] Xu T., Pruitt L., J. Mater. Sci: Mater. Med. 10 (1999) 83.

[23] Platon F., Fournier P., Rouxel S., Wear 250 (2001) 227.

[24] Dearnaley G., Arps J.H., Surf. Coat. Tecnhol. 200 (2005) 2518.

[25] Roy R.K., Lee K.-R., J. Biomed. Mater. Res: Part B – Appl. Biomater., in press

[26]Taeger G., Podleska L.E., Schmidt B., Ziegler M., Nast-Kolb D., Materialwissenschaft und Werkstofftechnik 34 (2003): 1094.

[27] Vila M., Carrapichano J.M., Gomes J.R., Camargo Jr. S.S., Achete C.A., Silva R.F., submitted to Wear.

[28] Hutchings I.M., Tribology: Friction and Wear of Engineering Materials, Butterworth-Heinemann, UK, 2003, pp. 15, 49, 50.

[29] Bellosi A., Guicciardi S., Tampieri A., J. Eur.. Ceramic. Soc. 9 (1992) 83.

[30] Voevodin A.A., Donley M.S., Zabinski J.S., Bultman J.E., Surf. Coat. Technol. 76-77 (1995) 534.

[31] Gomes J.R.,.Osendi M.I, Miranzo P., Oliveira F.J., Silva R.F., Wear 233-235 (1999) 222.

[32] Kokubo T., H. Takadama, Biomaterials 27 (2006) 2907.

[33] Hutchings I.M., Tribology—Friction and Wear of Engineering Materials, Ed. Butterworth-Heinmann, UK (2003)

[34] Vila M., Salgueiredo E., Amaral M.S., Fernandes A.J.S., Costa F.M., Cavaleiro A. Silva R.F., Diam. Rel. Mater. 15 (2006) 944.

[35] Vila M., Abreu C.S., Salgueiredo E., Almeida F.A., Fernandes A.J.S, Costa F.M., Gomes J.R., Silva R.F., Thin Solid Films 515 (2006) 2192.

[36] Gull R.M., FMcGarry.J., Bragdon C.R., Muratoglu O.K., Harris W.H., Biomaterials 24 (2003) 3193.

[37] Dumbleton J.H.. Tribology of natural and artificial joints. Tribology Series-3. Elsevier (1981).

Chapter IV

DLC-coated Si_3N_4-bioglass composite

(Adapted from "Hard a-C/DLC coatings on Si_3N_4-Bioglass composites", M. Vila, E. Salgueiredo, M.S. Amaral, A.J.S. Fernandes, F.M. Costa, A. Cavaleiro, R.F. Silva, Diamond and Related Materials 15 (2006) 944-947)

1. Introduction

Amorphous carbon/diamond-like carbon (a-C/DLC) films act as solid-film lubricants in wear-resistant parts of mechanical assemblies or as cutting tools, but also as protective coatings in implanted dental devices such as orthodontic archwires and artificial dentures. In these systems, a protective coating is needed as long as the active saliva corrodes Ni containing devices causing allergenic reactions due to Ni release [1,2]. Other fields of biomedical applications of a-C/DLC are blood contacting implants such as artificial hearts, [3] heart valves and stents that are already commercially available [4]. Furthermore, recent studies show that these films seem to be promising candidates for articulated implants as hip and knee joints [5]. The biocompatibility of these films has been widely studied in animal and human cell lines as well as its haemocompatibility and in all cases it has been reported to produce no significant levels of cellular toxicity [6]. Single or multilayered [1,7] DLC films are used to improve the prosthesis biotribological properties as long as they present chemical inertness, high hardness and low roughness, providing low friction and wear coefficients [8-11].

A novel biocomposite material, the Si_3N_4-bioglass, has been demonstrated to possess a good combination between the Si_3N_4 properties (fracture toughness, hardness, wear resistance, bioinertness) and the bioglass bioactivity [12,13]. These features make it a suitable material for prosthetic applications but could be improved by a DLC coating due to its auto-lubricant properties, as here proposed for the first time. The bioactivity of Si_3N_4-bioglass biocomposite inside the host bone ensures a good mechanical linkage, while the a-C/DLC coating of the prosthesis head reduces the friction in the working area.

The PVD techniques allow the growth of non-hydrogenated amorphous carbon films at lower deposition temperatures compared to CVD methods. The main problem of the former is the high intrinsic stress usually presented in hard coatings, that leads to poor adhesion, especially on Ti alloys, CoCrMo alloys and stainless steel, commonly used as prosthesis materials [14,15]. Some films have been prepared with the incorporation of impurities as Ti, B, Cu, Ag and V into the carbon network for lowering the stress, although keeping the hardness [16-19].

However, while these films allow the preparation of surfaces with antibacterial effect, doping is not recommended in human body implants because of the toxic reactions.

The chemical interaction between the film and the substrate surface also interfere in adhesion. This feature is beneficial when, for example, a carbide interlayer forms [20]. Si_3N_4 is a carbide former and this property may constitute an additional advantage for its use as a substrate for a-C/DLC growth. To reduce the DLC residual stress and improve adhesion, avoiding delamination, these films have been growth on heated substrates at medium temperatures (200ºC) [21] without any additional incorporation to the film network and without any substrate bias.

2. Experimental

The bioactive component of the Si_3N_4 composite as a similar composition to commercial glass Bioglass®45S5, with the chemical composition: $45.0SiO_2$-$24.5Na_2O$-$24.5CaO$-$6.0P_2O_5$ in wt%. The powders used for the preparation the bioglass are shown in Table 1.

Table 1: Powders used in the preparation of the bioglass

Compound	Reference	M(g/mol)
SiO_2	Quatz p.a., Merck	60.08
Na_2CO_3	Sodium Carbonate p.a., Merck	105.99
$CaCO_3$	Calcium Carbonate 99,0%, Panreac	100.087
$Ca(H_2PO_4)_2.H_2O$	Hydrated Calcium dihydrogen Phosphate, Merck	252.08

The powders were thoroughly mixed with isopropyl alcohol for 4h and dried. The powder was melted in an electric furnace at 1450 ºC for 2h in a platinum crucible. The thermal cycle is described in Figure 1.

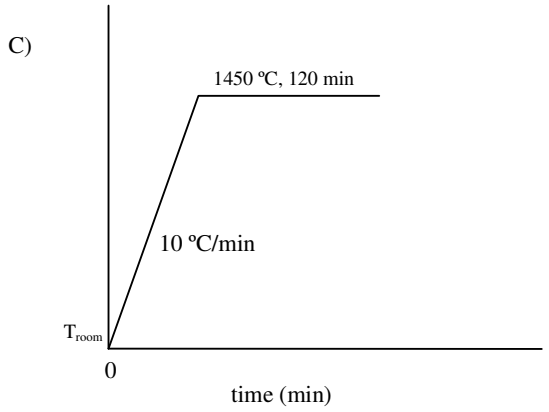

Figure 1: Thermal cycle for the fusion of the bioglass

The melt was poured into water, collected from the recipient and dried at 100 ºC. The bioglass was milled in an agate jar with agate balls for 24h, with isopropyl alcohol, until a final particle size of ~ 1.5 μm.

The bioactive powder was mixed with Si_3N_4 powder (Starck M11), in a 30-70% weight proportion. The powders were placed in an agate jar with agate balls in isopropyl alcohol and milled for 4h. After drying and sieving with a 45 μm mesh, the composite powder was placed in a boron nitride coated graphite die and densified by uniaxial hot pressing, HP.

The hot pressing cycle was: heating rate of 10 ºC/min up to a fixed temperature of 1350 ºC, followed by a stage of 40 min at this temperature, under an applied pressure of 30 MPa.

With this technique that combines temperature and pressure, dense substrates (> 96%) were obtained. The temperature was chosen bearing in mind that the decomposition of the bioglass must be avoided. These dense substrates possess good mechanical properties and low porosity, essential parameters for biotribological applications.

Prior to DLC deposition, the substrate plates were polished by a sequence of diamond pastes until colloidal silica (0.25 μm) finishing.

The DLC films were grown over Si_3N_4–bioglass 8 ×8×3 mm^3 samples by using a planar 3'' magnetron sputtering source operated by a DC power supply with no applied substrate bias voltage. A circular graphite target with a thickness of 3 mm was clamped to the water-cooled electrode. The substrate material was heated up to 200ºC. The vacuum system provided a residual pressure near 1×10^{-6} mbar. Using Ar as sputtering gas at a working pressure of 5×10^{-3} mbar and a DC power of aprox. 20 W, the obtained a-C/DLC growth rate was typically 4nm/min.

Film and substrate microstructural information was assessed by AFM (Digital Instrument Multimode IIa) and micro-Raman spectroscopy (Jobin-Yvon T64000, Ar^+ 514.5 nm, ~1μm spot size). The film thickness was measured by SEM (Hitachi 4100S).

Ultramicrohardness equipment from Fisher Instruments (Fischerscope H100) was used for the hardness and Young's modulus measurement. A nominal load of 10 mN was applied, with resolution better than 1 mN.

Measurement of the indentation depth was achieved with a capacitance displacement gauge of 2-nm accuracy. During the test, the load is increased in steps until

the nominal test load is reached. The number of steps was 60 and the time between them was 0.5s. The first load step was always equal to 0.4 mN. For subsequent steps, the value of the load increments between two consecutive steps ($\Delta P=P_i - P_{i-1}$) is such that the difference ($(P_i)^{0.5} - (P_{i-1})^{0.5}$) is constant during them loading period. During unloading, the same steps were used. Two creep periods were allowed during the tests: at maximum load and at the lowest load during unloading (0.4 mN). Each creep period was of 30 s. The experimental loading/unloading curve results were corrected forward to minimise the effects of the uncertainties related to the indenter shape, the thermal drift of the equipment and the surface roughness at both the indentation depth measurements and the zero position of the indentation depth. The hardness and the Young's modulus were calculated from the corrected data following the procedure indicated somewhere else [22]. Each value was an average of at least 10 indentations at ten different locations after checking that hardness was independent of load for this range of contact depths.

3. Results and discussion

The surface morphology of the Si_3N_4-bioglass composite substrate is shown in Figure 2a). Due to the relatively low hot-pressing temperature, the final microstructure is mainly formed by very small unreacted α-Si_3N_4 equiaxial grains, embedded in the bioglass matrix. The as-polished substrate surface roughness is Ra=3.2 nm. After coating, the surface smoothes down to an extremely low value of Ra=2.6 nm (Figure 2b).

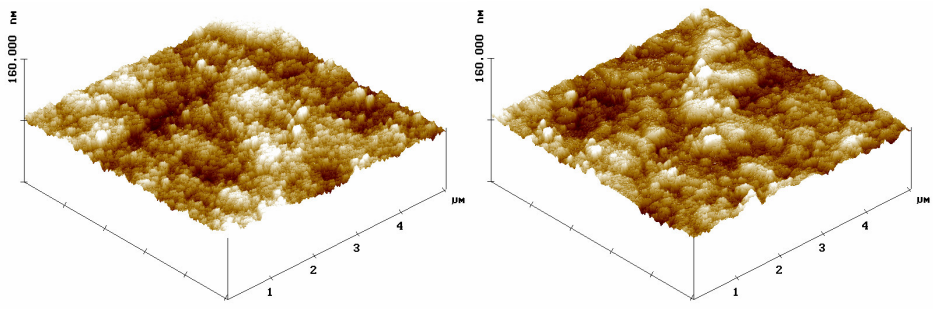

Figure 2: AFM images of surface morphology: (a) substrate and (b) a-C/DLC film.

A fractured section of the coated material is presented in Figure 3. Both the AFM and SEM micrographs reveal a continuous layer of carbon agglomerates covering the substrate, without any evidence of macroparticles or droplets that used to result in other techniques such as vacuum arc discharge [23].

The a-C/DLC films are dense and homogeneous in all the deposition area with no columnar growth, with a thickness of aprox. 0.7 μm (Figure 3) They do not present spontaneous delamination as happened with films previously grown without substrate heating and other deposition parameters as higher DC power or thicker films (over 1μm).

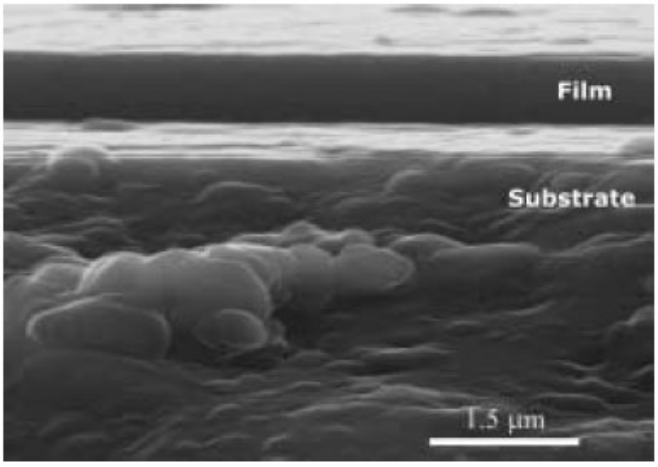

Figure 3: Cross-sectional SEM image of a fracture surface showing the a-C/DLC film and the substrate

Figure 4 shows a representative Raman spectrum of these films. Two well-known broad bands characteristic of disordered carbon films dominate the plot. A fitting was made with a BWF (Breit-Wigner-Fano) line shape for the G peak and a Lorentzian for the D peak [21].

The prominent G band, corresponding to the sp^2 C-C stretching modes, appears located at ~1555 cm^{-1}, while a much less intense D band, corresponding to the breathing mode of sp^2 coordinated rings, locates at ~1350 cm^{-1}.

The downshift on the G band position relative to the 1580 cm^{-1} zone centre graphite peak is generally indicative of an increase of sp^3 content, while the weak intensity of the D band denotes reduced clustering. These features usually correlate well with good mechanical properties, such as high hardness.

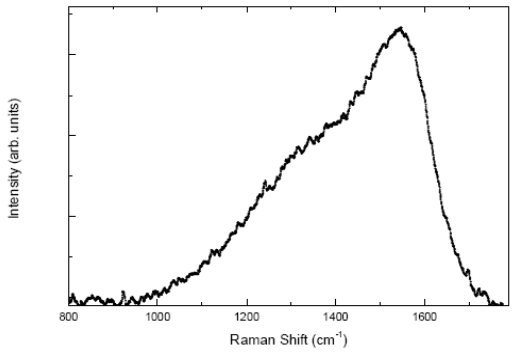

Figure 4: Micro – Raman spectrum of the a-C/DLC layer

The substrate micro-hardness and elastic modulus were reported elsewhere [7] giving values of 10.3 GPa and 197 GPa, respectively.

Ultra-microhardness measurements reveal that the a-C/DLC coating significantly increases the surface hardness to 16.3 GPa. On the contrary, the elastic modulus of the film, E=156 GPa, is lower than the substrate itself. The obtained values follow the relationship between hardness and Young Modulus, H>E/10, empirically deduced for DLC film designation [24]. These data were determined from indentation load-depth curves as the one shown in Figure 5. It is worth to note that under a maximum load of 10 mN, the indentation depth attains a value of 0.16 μm, corresponding to 22% of the film thickness, the threshold of the substrate influence on the film hardness [25]. So, no discontinuities appear in the load-depth curve. Moreover, the uniformity of the curve profile denotes the tough nature of the film.

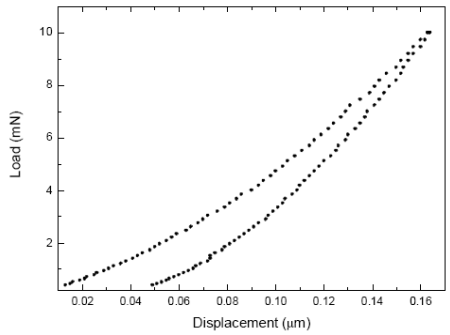

Figure 5: Load vs indentation depth curve of the 0.7 μm thick a-C/DLC film

Graphite structure, the main constituent of the present amorphous carbon films, present low hardness due to the easy sliding of the basal planes (002) relative to each other and to grain sliding along the grain boundaries. Film growth by sputtering at high vacuum allows a dense amorphous structure to be obtained with low impurity content and small cluster size [26].

Bias application in the substrate also enhances film density that leads to a high stress accumulation into the film, increasing the hardness, but can provoke the peeling off of the substrate. It has been reported that a high hardness is not only a consequence of a high sp^3 content in the amorphous carbon film but also of their nanostructure. The combination of these features results in a wide range of hardness values for the a-C/DLC films grown by sputtering, from 5 GPa [27] to 45 GPa [18]. The best values, of the same magnitude of those obtained by filtered arc deposition techniques [2], are obtained with substrate bias application, but a high hardness of 25 GPa was reported for a-C films grown on Si by sputtering without bias [28]. However, it must be taken into account that hardness is influenced by the measurement technique, thus micro-hardness and nanohardness may give different values for the same sample [21].

The hardness of the present biocomposite coated material is slightly higher than the value of 14.2 GPa obtained for a competitor material for orthopaedic applications, a PECVD-DLC coated alumina [28].

When compared to the most commonly used prosthetic titanium, stainless steel and Ti alloys, the hardness of the a-C/DLC material here presented corresponds to more than a two fold increase (6.5, 5.5 and 8.5 GPa [2], respectively), despite no substrate bias applied.

These films have the advantage of improving the surface properties of this biomaterial, acting as autolubricants while improving hardness. Moreover, having a lower elasticity modulus than the substrate itself, a higher toughness is provided, which is requirement for the tribological behaviour of biomedical applications like articulated solid implants.

4. Conclusions

Si_3N_4-bioglass bioceramics were successfully coated with DLC films prepared by sputtering with no substrate bias application. Well adhered films were obtained with

substrate heating at 200ºC. Films are dense and homogeneous in all the deposited area with an extremely low roughness of 2.6 nm.

The film nanostructure, confirmed by the weak intensity of the Raman spectra D band position, combined with significant sp^3 content, as depicted by the G band downshift, lead to a hardness value of 16.3 GPa, as estimated by ultramicrohardness measurements.

These films have the advantage of improving the surface properties of this biomaterial, acting as autolubricants while improving hardness. Moreover, having a lower elasticity modulus than the substrate itself, a higher toughness is provided, which is requirement for the tribological behaviour of biomedical applications like articulated solid implants.

References Chapter IV

[1] Kobayashi S., Ohgoe Y.,. Ozeki K., Sato K, Sumiya T.,. Hirakuri K.K, Aoki H., Diam. Rel. Mater. 14 (2005) 1094.

[2] Sheeja D.,. Tay B.K,. Shi X., Lau S.P., Daniel C., Krishnan S.M., Nung L.N., Diam. Rel. Mater. 10 (2001) 1043.

[3] Ohgoe Y, Hirakuri K.K., Tsuchimoto K., Friedbacher G., Miyashita O., Surf. Coat. Tech. 184 (2004) 263.

[4] Hauert R., Diam. Rel. Mater. 12 (2003) 583.

[5] Loir A.S, Garrelie F., Donnet C., Rogemond F., Subtil J.L., Forest B., Belin M., Laporte P., Surf. Coat. Tech. 188-189 (2004) 728.

[6] Jones M.I., McColl I.R., Grant D.M., Parker K.G., Parker T.L., Diam. Rel. Mater. 8 (1999) 457.

[7] Lu W., Komvopoulos K., Patsalas P., Charitidis C., Gioti M., Logothetidis S., Surf. Coat. Tech. 168 (2003) 12.

[8] Jun.Q. Tribol. Lett. 14 (2) (2003) 105.

[9] Camino D., Jones A.H.S., Mercs, D., Teer G., Vacuum, 52 (1999) 125.
D.
[10] Hench L, J. Am. Ceram. Soc. 1998; 81 (7) (1998) 1705.

[11] Tiainen V. M., Diam. Rel. Mater. 10(2001) 153.

[12] Amaral M.,.Lopes M.A, Silva R.F., Santos J.D., Biomaterials 23 (2002) 857.

[13] Santos J. D., Key Eng Mater, 192-195 (2001) 589.

[14] Dowling D.P., Kola P.V., Donnelly K., Kelly T.C., Brumitt K., Lloyd L., Eloy T., Therin M., Weill N., Diam. Rel. Mater. 6 (1997) 390.

[15] Lappalainen R., Heinonen H., Anttila A., Santavirta S., Diamond Rel. Mater. 7 (1998) 482.

[16] Hauert R., Diam. Rel. Mater. 12 (2003) 583.

[17] Chhowalla M., Yin Y., Amaratunga G.A.J.,. McKenzie D.R, Th. Frauenheim. Appl. Phys. Lett. 69 (16) (1996) 2344.

[18] Franceschini D.F., Achete C.A.,.Freire Jr F.L., Appl. Phys. Lett. 60 (26) (1992) 3299.

[19] Bauer C., Leiste H., Stüber M., Ulrich S., Holleck H., Diamond Rel. Mater 11 (2002) 1139.

[20] Morshed M.M., Cameron D.C.,.McNamara B.P,. Hashmi MS.J., Surf. Coat. Tech 174-175 (2003) 579.

[21] Robertson J., Mater. Sci. Eng. R 37 (2002) 129.

[22Antunes] J.M., Cavaleiro A., Menezes L.F., Simões M.I., Fernandes J.V., Surf. Coat. Technol. 149 (2002) 27.

[23] Fukui H., Okida J., Omori N., Moriguchi H., Tsuda K., Surf. Coat. Tech. 187 (2004) 70.

[24] Schneider D., Meyer C.F., Mai H., Schöneich B., Ziegele H., Scheibe H.J., Lifshitz Y., Diamond Relat. Mater. 7 (1998) 973.

[25] Xu Z., Rowcliffe D., Surf.Coat.T echnol.161 (2002) 44.

[26] Kulikovski V.Y., Fendrych F., Jastrabik L., Chostova D., Soukup L., Pridal J., Franc F.., Diam. Rel. Mater 12 (2003) 1378.

[27]. Santos L.V, Trava-Airoldi V.J., Corat E.J., Iha K., Massi M., Prioli R., Landers R., Diamond Rel. Mater. 11 (2002) 1135.

[28] Kulikovski V., Bohac P., Franc F., Deineka A., Vorlicek V., Jastrabik L., Diamond Relat. Mater. 10 (2001) 1076.

[29] Christiansen S.. J Mater Res.11 (8) (1996) 1934.

Chapter V

Conclusions

DC magnetron sputtering proved to be an adequate technique to obtain DLC coated silicon nitride (Si_3N_4) ceramics aiming articular prosthesis applications. The optimal deposition conditions regarding the best adhesion levels must be selected depending on the substrates composition: i) for bulk Si_3N_4, a Si interlayer is required; ii) for Si_3N_4/TiN conductive composites, a negative bias voltage should be applied; iii) for Si_3N_4/bioglass composites, substrates should be heated to 200ºC. DLC films were dense and homogeneous in all the deposited area, showing extremely low surface roughness values of about 2.6 nm (RMS). DLC coatings have high significant sp^3 content confirmed by the ratio between Raman spectra G and D graphitic bands, leading to a hardness value of 16.3 GPa.

Surface characterization included the evaluation of the zeta potential and surface charge of the coating. The zeta potential of -35.0±1.3mV indicates that the DLC coatings are only slightly negative charged. DLC coating is quite hydrophobic, with a total surface tension of 45.7mN/m, presenting a minor polar component (9.1mN/m). DLC showed no apatite layer formation ability in *in vitro* testing using an acellular simulated body fluid (SBF). Biocompatibility assays using MG-63 osteoblast-like cells demonstrated the absence of toxicity of the DLC coatings. Cells presented a normal morphology and higher cell growth rate compared to standard culture plates, although with low cell adhesion. This is a very favourable result, considering the specific application of articulated implants, in which cell adhesion is undesirable.

Biotribological characterization was performed to evaluate the level of adhesion and friction coefficient values of the DLC-coated Si_3N_4 substrates in self-mated tests and DLC-coated Si_3N_4 balls against Si_3N_4/TiN substrates. For the homologous pairs, the film presented premature delamination at low loading conditions (3 N, 0.97 GPa). Applying a negative bias voltage to a conductive Si_3N_4/TiN composite offered a significant improvement in the tribological behaviour of the film. A very low friction coefficient value of ~ 0.015 was obtained during the full duration of the test. The Si interlayer deposition prior to the DLC coating on Si_3N_4 bulk substrates revealed superior adhesion in reciprocating sliding experiments against UHMWPE balls. DLC-coated surfaces presented no wear marks or polymer transfers, while in the UHMWPE balls the wear scars were

unmeasurable. Comparing the dry sliding conditions with SBF lubricated experiments, the first presented a higher friction coefficient (0.25), significantly reduced by the SBF lubrication (0.02).

The favourable results in terms of biocompatibility and biotribology obtained for the DLC-coated Si_3N_4 ceramics present an interesting insight for applications in articulated joint prostheses.

In the future, more extended biocompatibility tests should be conducted using osteoblast and fibroblast cells, regarding adhesion and proliferation. Tribological tests using a joint simulator are imperative to evaluate the coating and substrate performance. The joint simulator reproduces, as closely as possible, the physiological motion, loading and environment of the joint.